Coordination Chemistry Reviews 255 (2011) 357–373

Contents lists available at ScienceDirect

Coordination Chemistry Reviews

journal homepage: www.elsevier.com/locate/ccr

Review

Periodic one-dimensional nanostructured arrays based on colloidal templates, applications, and devices

Yue Li[a,b,*], Naoto Koshizaki[b], Weiping Cai[a,*]

[a] Key Laboratory of Materials Physics, Anhui Key Laboratory of Nanomaterials and Nanotechnology, Institute of Solid State Physics, Chinese Academy of Sciences (CAS), Hefei 230031, Anhui, China

[b] Nanosystem Research Institute (NRI) National Institute of Advanced Industrial Science and Technology (AIST) Central 5, 1-1-1 Higashi, Tsukuba, Ibaraki 305-8565, Japan

Contents

ARTICLE INFO

Article history:
Received 9 July 2010
Accepted 26 September 2010

Keywords:
Periodic array
Colloidal monolayer
One-dimensional nanostructure
Template
Mask
Device

ABSTRACT

A novel approach to fabricate periodic one-dimensional (1D) nanostructured arrays is developed using monolayer colloidal crystals as templates or masks. This approach is more flexible and less costly than traditional lithographic techniques. The morphology and structural parameters of periodic arrays can be easily controlled, further resulting in optimized properties. Herein we introduce recent work to create periodic 1D nanostructured arrays by combining colloidal templates with other techniques, such as solution techniques, electrodeposition, wet chemical etching, reactive ion etching (RIE), pulsed laser deposition (PLD), and sputtering. These periodic 1D nanostructured arrays with controllable morphology and structural parameters have extensive applications in areas such as nanophotonics, field emitters, solar cells, light-emitting diodes, and microfluidic devices.

* Corresponding author at: Key Laboratory of Materials Physics, Anhui Key Laboratory of Nanomaterials and Nanotechnology, Institute of Solid State Physics, Chinese Academy of Sciences (CAS), Hefei 230031, Anhui, China. Tel.: +86 551 5591465.
E-mail addresses: yueli-ri@aist.go.jp (Y. Li), wpcai@issp.ac.cn (W. Cai).

0010-8545/$ – see front matter © 2010 Elsevier B.V. All rights reserved.
doi:10.1016/j.ccr.2010.09.015

1. Introduction

One-dimensional (1D) nanostructures (e.g., nanowires, nanorods, and nanotubes) exhibit novel properties, depending on dimensional and size reduction, in magnetics, electrical as well as thermal transport and hence have been intensively investigated [1–4]. If 1D nanostructures can be organized into periodic arrays, their applications will be extended to many devices (e.g., biosensors, photonic crystals, microfluidic devices, and electrochemical devices). Most of their properties are morphology- and arrangement-parameter-dependent; therefore, the fabrication of 1D nanostructured arrays with controlled morphologies and structures becomes more important on a large scale. The most widely used techniques are conventional lithographies, including photolithography, electron-beam lithography, scanning tunneling microscopy, and atomic force microscopy lithography [5–10]. Photolithography has the disadvantage of low resolution because it cannot be widely applied due to its diffraction-limited resolution, about $\lambda/2$ (λ is photo-wavelength). Therefore, it cannot be widely used in nanostructural fabrication [5]. Other lithography methods (e.g., electron-beam lithography, scanning tunneling microscopy, and atomic force microscopy lithography) have the ability to create high-quality 1D nanostructured arrays; however, most laboratories cannot afford them because of their high costs and low sample throughput. Besides lithography, anodic aluminum oxide (AAO) templates are often applied to fabricate 1D nanostructured arrays [11,12]. This method has the advantages of low cost, high aspect ratio, and good repetition; however, these 1D nanostructured arrays need the support of AAO templates. If the templates are removed, the 1D nanostructured units aggregate with each other and may even collapse; thus, their application in nanodevices is seriously restricted.

With the development of colloidal science in the past few decades, researchers have successfully prepared highly monodisperse colloidal spheres with a size deviation of less than 5% (e.g., polystyrene (PS), silica, and PMMA) in liquid media by different methods [13–15]. The synthesis of monodisperse colloidal spheres provides the opportunity to extend their applications. Scientists have found that monodisperse colloidal spheres can self-assemble into periodic sphere arrays, called colloidal crystals, with hexagonal arrangement by well-controlled experimental conditions using drop-coating [16–18], spin-coating [19–22], dip-coating [23–27], electrophoretic deposition [28–31], and self-assembly at the liquid/gas interface [32–34]. The successful achievement of colloidal crystals paves the way for their use as templates to fabricate ordered structured arrays [35–37]. If the colloidal crystal is controlled to only one layer (monolayer) on the substrate during preparation, it will be very helpful to devise and fabricate the periodic arrays with well-defined nanostructures based on such colloidal templates. Since Deckman and Dunsmuir fabricated a periodic column array by the monolayer colloidal crystal (called colloidal monolayer) as a mask using natural lithography in 1982 [38], the colloidal monolayer template technique has been developed as a very flexible method to create two-dimensional (2D) periodic arrays (e.g., nanoparticle arrays [39–44], nanohole arrays [45,46], nanopore arrays [47–56], nanobowl arrays [57–61], and nanoring arrays [62,63]) with controllable morphologies. Interestingly, in addition to these periodic arrays, 1D nanostructured periodic arrays (e.g., nanotube, nanopillar, and nanorod arrays) can be fabricated based on direct or indirect colloidal monolayer templates by different methods, such as chemical vapor deposition (CVD), sputtering deposition, pulsed laser deposition (PLD), chemical etching, reactive ion etching (RIE), and electrochemical deposition. The morphologies and sizes of these 1D nanoobjects in the periodic arrays are easily controlled by colloidal monolayer templates with different periodicities; therefore, their properties that are dependent on morphology and size can be optimized. This method of creating 1D nanostructured arrays has the advantage of low cost. The novel properties optimized by parameters have many applications in nanophotonics, field emitters, nanogenerators, optical devices, sensors, and nano-biotechnology.

In this review, we focus mainly on recent developments of the colloidal monolayer template technique to create 1D nanostructured arrays and the following applications of such periodic arrays: (1) one-step strategies based on colloidal monolayer templates to 1D nanostructured arrays, including nanorod arrays on the colloidal monolayers by oblique deposition or glancing angle deposition (GLAD), nanopillar arrays based on heat-deformed colloidal monolayer templates or masks by sol–gel/solution dipping deposition and electrochemical deposition; (2) multiple-step strategies to periodic 1D nanostructured arrays. Based on colloidal monolayer templates or masks, the nanoparticle, nanopore, as well as nanoplate patterns can be first fabricated, which can be further used as templates or masks to prepare the 1D nanostructured arrays by reactive ion etching, chemical vapor deposition, sputtering deposition and wet chemical etching; (3) applications and devices of periodic 1D nanostructured arrays with morphology-dependent properties.

2. One-step strategies based on colloidal monolayer

Pristine or heat-deformed colloidal monolayers can be directly used as templates or masks to fabricate 1D nanostructured periodic arrays, combined with other techniques (e.g., oblique deposition or glancing angle deposition (GLAD), solution dipping, electrodeposition, and reactive ion etching (RIE)). Here we introduce methods of creating nanorod arrays on a colloidal monolayer by oblique deposition or GLAD, hierarchical micro/nanorod arrays by elec-

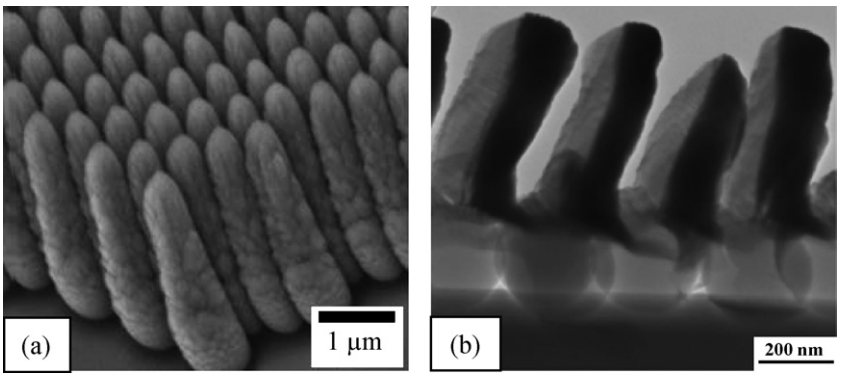

Fig. 1. (a) Si nanopillar array on a colloidal monolayer produced by GLAD. Reprinted with permission from Ref. [64]. Copyright 2006 Elsevier. (b) Si–Ta two-component nanorods grown on a silica colloidal monolayer by SO-GLAD. Reprinted with permission from Ref. [65]. Copyright 2008 Elsevier.

trodeposition, nanopillar arrays based on a heat-deformed colloidal monolayer by sol–gel/solution deposition or electrodeposition, and periodic nanorod arrays by RIE.

2.1. Nanorod arrays on the colloidal monolayer by oblique deposition or GLAD

2.1.1. Single deposition direction in high vacuum

Utilizing physical deposition (e.g., sputtering, thermal evaporation, and PLD), if the deposition chamber provides a good vacuum condition, the incident vapor or ejected species maintains a single direction for the deposition from the target to the substrate. When a colloidal monolayer is applied as the substrate, vertical or titled nanopillar arrays can be fabricated on the top of the colloidal monolayer due to the shadow effect [64–71]. By changing the angle between the substrate normal and the direction of the incident vapor as well as the rotation speed of the substrate, one can readily create vertical nanopillar arrays on the colloidal monolayer by GLAD. Gall and co-workers deposited Si onto a colloidal monolayer from an angle R of 72° with respect to the surface normal; the substrate was rotated about the polar axis at a speed of 60 rpm, and Si nanopillar arrays were fabricated on the colloidal monolayer (Fig. 1a) [64]. By simultaneous opposite glancing angle deposition (SO-GLAD), Gall and co-workers also used two different

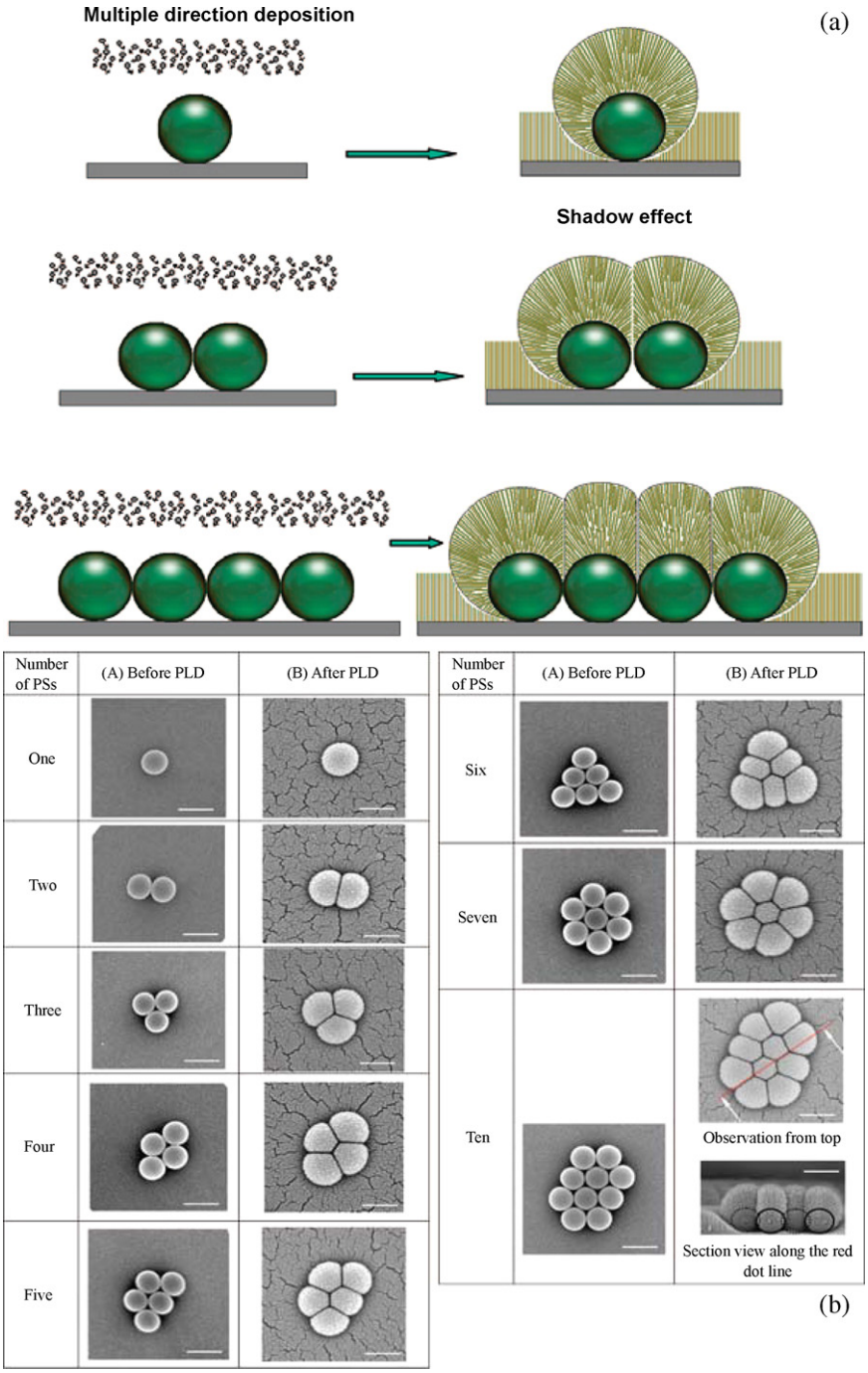

Fig. 2. (a) Formation mechanism of hcp nanorod arrays under high background gas pressure. (b) Morphologies before and after TiO_2 PLD on a PS sphere cluster surface with different sphere numbers (scale bars are 500 nm).
Reprinted with permission from Ref. [72]. Copyright 2008 American Chemical Society.

materials for deposition simultaneously from oblique angles from opposite sides onto colloidal monolayers. Selective deposition was obtained by atomic shadowing on only the side that was exposed to the deposition flux, leading to nanopillar growth where each rod consisted of two laterally separated components (Fig. 1b) [65].

2.1.2. Multiple direction deposition in high background gas pressure

In physical deposition, if background gas at high pressure is introduced into the deposition chamber, the movement direction of the ions, electrons, and molecules of the species ejected from targets changes from an almost uniform direction to multiple directions, due to collisions among them. When a colloidal monolayer substrate is used for deposition, it is easy to achieve an ordered nanorod array on the colloidal monolayer under multiple direction deposition and shadow effects of colloidal spheres (Fig. 2a) [72]. The mechanism of such a formation is traced by combining the colloidal clusters with different sphere numbers and PLDs [72]. If one colloidal sphere is completely surrounded by the others, a nanorod forms on this sphere top, due to the multiple-direction deposition and shadow effect between neighboring spheres (Fig. 2b). This result implies that a nanorod array is easily formed after PLD if a colloidal monolayer with a large area is used. This nanorod has a very rough structure on the surface and is composed of many nanobranches, indicating porous structures with high specific surface area (Fig. 3) [72].

In this case, the nanorods always grow vertically and their growth direction is irrelevant to the substrate position with respect to the target. Their only distinctiveness is a different growth ratio at various positions of the substrate, due to the plasma plume shape in higher background gas pressure.

With this approach, besides amorphous TiO_2, nanorod arrays of other materials (e.g., amorphous WO_3, Co_3O_4, C, crystalline CuO, Fe_2O_3, and ZnO) can also be created [73–75].

The porosity and specific surface area of the nanorods can be tuned by varying the background gas pressure [76,77]. The porosity and surface area increase with increase of background gas pressure (Fig. 4a–c) [76]. Crystalline anatase TiO_2 nanorod arrays could then be crystallized by annealing the amorphous TiO_2 nanorod arrays at 650 °C for 2 h, and the PS spheres under nanorods were entirely burned out. At the same time, the amorphous TiO_2 nanorods on the PS sphere tops changed to anatase TiO_2 and dropped vertically down to the original positions of the PS spheres in this annealing process. The volume of the TiO_2 nanorod decreased during this process; hence, a hexagonal non-closed packed (hncp) nanorod array formed from the pre-existing hexagonal closed packed (hcp) amorphous TiO_2 array. The resultant film adhered tightly to the substrate after annealing. It could not be detached from a substrate even after ultrasonication in water over 30 min. This result guarantees its reliable application for use as a field emitter. Because the porosity increase with increasing background gas pressure, the distance between neighboring anatase nanorods can be tuned with different background gas pressures in an hncp array after annealing. The distance will increase with increasing background gas pressure (Fig. 4(a′–c′) and (a″–c″)).

2.2. Hierarchical micro/nanorod arrays by electrodeposition

If a conductive layer (e.g., a thin layer of Au) is added on the surface of the colloidal monolayer, the aligned nanorods can grow on the colloidal sphere surface by electrodeposition, and a special hierarchical micro/nanorod array based on the colloidal monolayer template can be obtained [78,79]. Elias et al. first prepared a colloidal monolayer on cleaned FTO glass by self-assembly; then the FTO glass was immersed for 30 min in aqueous solution of $ZnCl_2$ with a high concentration of 2 M in order to obtain a thin conductive layer on the PS sphere surface by interaction between the carboxylate groups of the PS microspheres and the zinc precursor

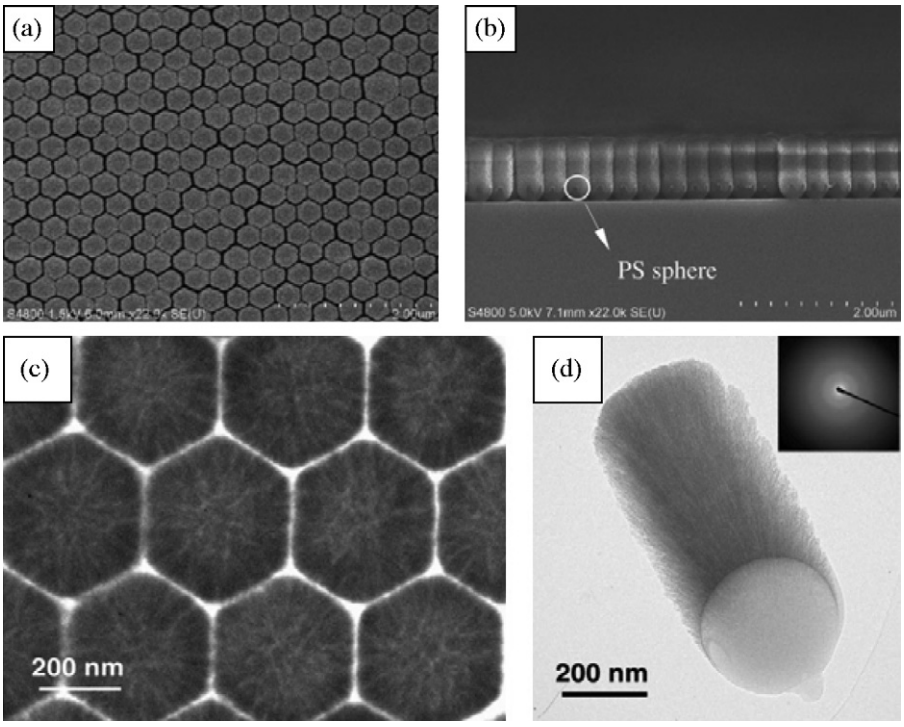

Fig. 3. Amorphous TiO_2 hcp nanorod arrays on a colloidal monolayer under higher background gas pressure produced by PLD. (a) SEM image of a nanorod array observed from the top. (b) SEM images of a single nanorod observed from the side.
Reprinted with permission from Ref. [72]. Copyright 2008 American Chemical Society.

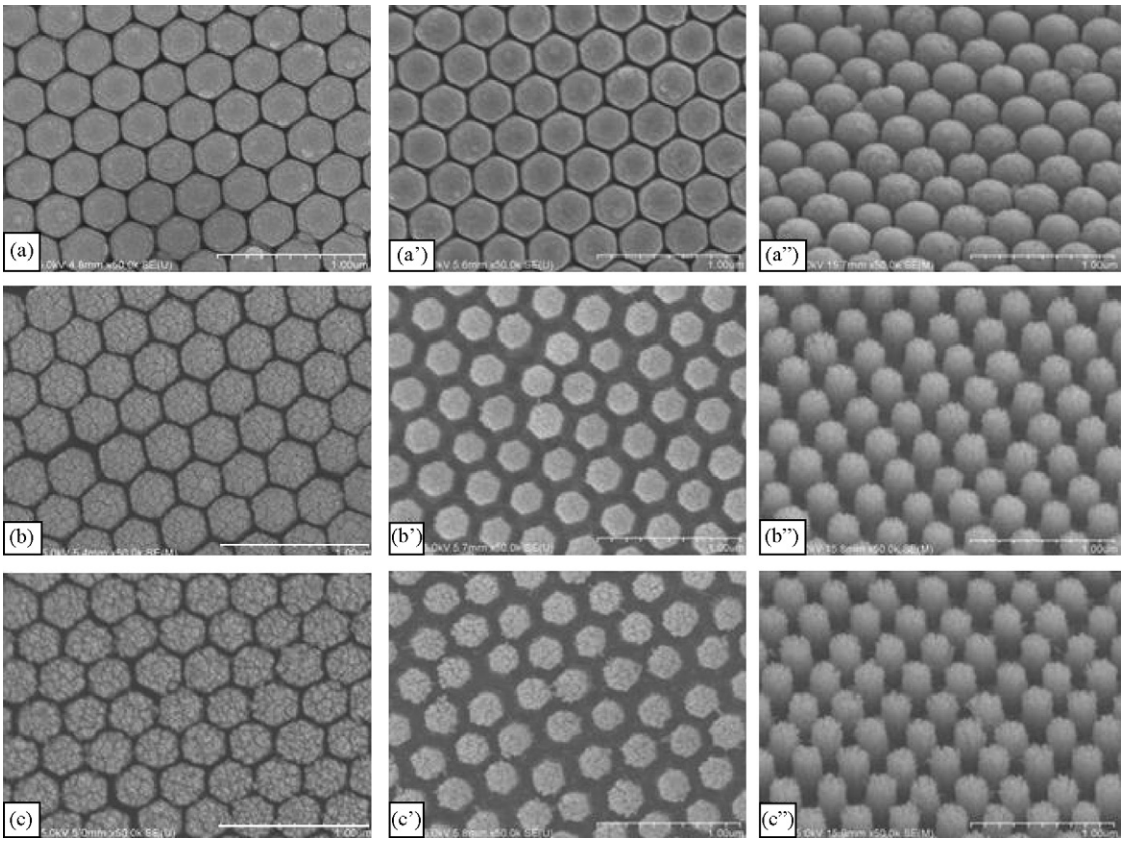

Fig. 4. FE-SEM images of an amorphous hcp TiO_2 nanorod array and anatase hncp TiO_2 nanorod arrays obtained by PLD under different background gas pressures and subsequent annealing. PLD was performed in oxygen (a) at 2.0 Pa for 200 min; (b) at 16.8 Pa for 43 min; (c) at 26.8 Pa for 30 min. (a–c) before annealing, (a′–c′) top views after annealing, (a″–c″) tilted view with 45° angle after annealing.
Reprinted with permission from Ref. [76]. Copyright 2009 Wiley-VCH.

[78]. Next this colloidal monolayer with a conductive layer on top was used as a working electrode in a three-electrode electrochemical cell, with a Pt spiral wire as the counter electrode and a saturated calomel electrode as the reference electrode for ZnO electrodeposition. After electrodeposition, the PS spheres were removed with toluene or burned off in air at 450 °C for 1 h. Thus, a hierarchical ZnO micro/nanorod array (e.g., hollow urchin-like array) was fabricated on a conductive substrate (Fig. 5). With this approach, the crucial point for the formation of these special structures is the treatment of PS with a high-concentration zinc precursor to prepare a conductive layer on the PS sphere surface. This step guarantees successful ZnO electrodeposition on PS sphere surfaces. Duan et al. developed an alternative method to create similar structures; they directly deposited an Au layer on the surface of a colloidal monolayer on ITO glass by sputtering, and this colloidal monolayer was applied as a working electrode for electrodeposition. Hierarchical micro/nanostructured arrays were also synthesized [79].

2.3. Short nanorod or nanopillar arrays based on heat deformed colloidal template

When the polymer colloidal monolayer on the substrate is heated at a temperature (e.g., 120 °C for PS) above glass transition temperature T_g (T_g of PS = 100 °C) for a certain time, the colloidal sphere surface melts slightly, and polymer spheres in the colloidal

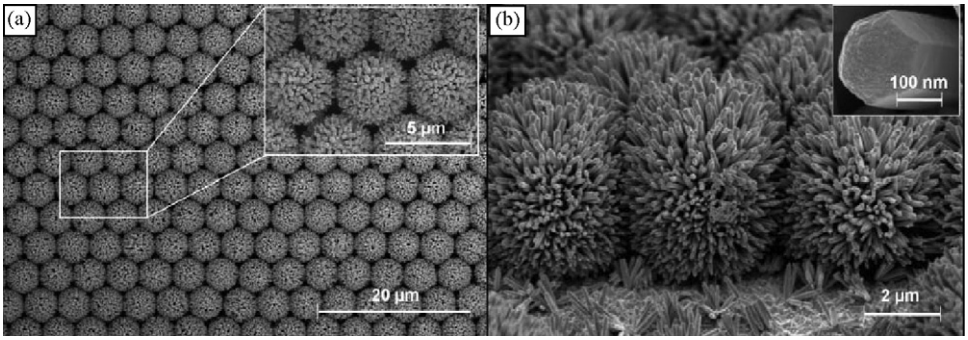

Fig. 5. ZnO hierarchical micro/nanostructured array produced by electrodeposition based on the colloidal monolayer after removal of PS. (a) Top view: the inset is a higher magnification. (b) Tilted view with an angle of 70°. The inset is a high-magnification SEM image nanorod embedded in the hierarchical micro/nanostructured unit.
Reprinted with permission from Ref. [78]. Copyright 2010 Wiley-VCH.

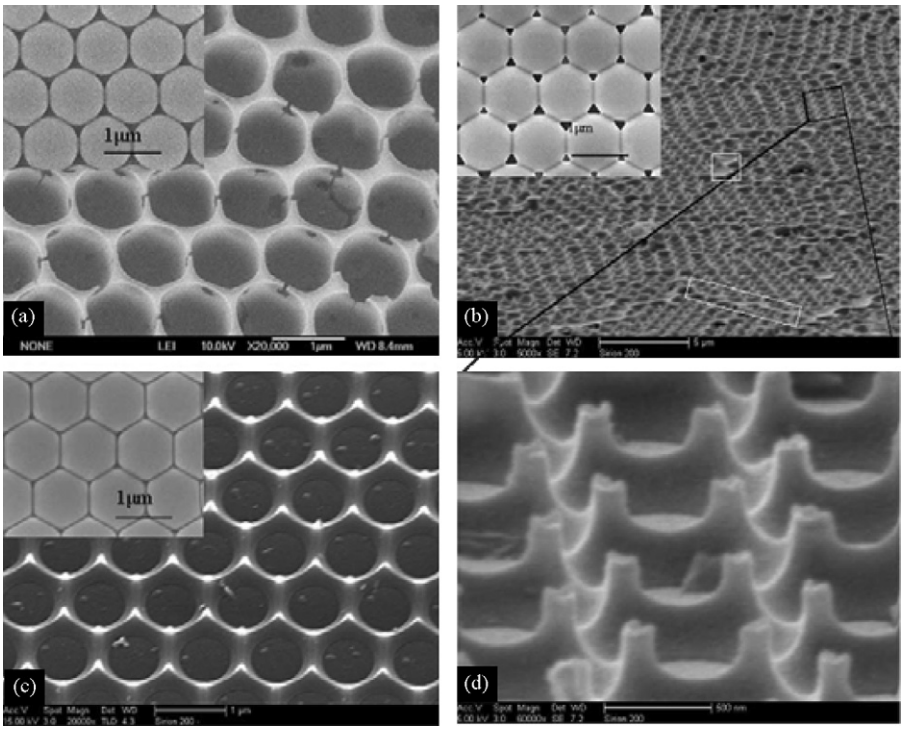

Fig. 6. FE-SEM images of Fe_2O_3 ordered structures fabricated with $Fe(NO_3)_3$ precursor solution, based on monolayer polymer colloid crystal with 1000 nm PSs in diameter heated for different times at 120 °C. The insets in (a, b, and d) are colloidal crystal heated for 0 min, 15 min, and 25 min, respectively. (a, b, and d) Corresponding periodic nanostructures prepared using such templates. (c) Local magnification of (b).
Reprinted with permission from Ref. [80]. Copyright 2005 Elsevier.

monolayer are so deformed that triangular prism channels can be formed at the interstices among them [80–88]. In addition to the methods described above, nanopillar arrays have been synthesized using the triangular channels of the heat-deformed colloidal monolayer. This monolayer can be used as a template to fabricate some special nanostructured arrays (e.g., nanorod or nanopillar array). By such templates, periodic nanopillar arrays of silica, Fe_2O_3, and ZnO have been created by solution/sol-dipping deposition, and electrodeposition, solution growth.

The appropriate heating time of the polymer colloidal templates is a key factor in the heat-deformed colloidal template strategy. For instance, ordered hcp pore arrays with the pore shape of a truncated hollow sphere can be obtained with a heating time of 0 min, which agrees well with the pristine colloidal template (Fig. 6a). Interestingly, when such polymer monolayer colloidal crystals are heated at 120 °C for 15 min, their morphologies exhibit a large change. Due to heating at a temperature above the glass transition of PSs, the PSs are obviously deformed, leading to contact evolution between neighboring PSs from quasi-point contact to facet contact. Therefore, interstices among the PSs in the colloidal monolayer become smaller from the top view, and triangular-shaped channels are formed among the PSs (Fig. 6b and c). However, when the polymer colloidal is overheated, the channels almost disappear in the templates. Correspondingly, the morphology takes on a regular network, and no pillars are found, due to the lack of channels in the overheated template (Fig. 6d).

Besides solution/sol-dipping deposition, other methods (e.g., electrodeposition and solution growth) can be used to prepare 1D nanostructured arrays, based on the heat-deformed colloidal templates. Zeng et al. developed a method to synthesize patterned ZnO nanorod arrays by electrodeposition, based on such templates [81]. A deformed colloidal monolayer with an Si substrate was employed as the cathode and zinc foil as the anode to perform electrodeposition at a constant current density in the electrolyte. After the colloidal monolayer template was removed, a ZnO nanorod array formed at the substrate. Using the deformed colloidal monolayer on the zinc foil by microwave heating as a mask, Qi et al. grew ZnO nanorods in the channels in the deformed monolayer by chemical growth in the reacting agents of $Zn(NO_3)_2$ and hexamethylenetetramine aqueous solution [82–84].

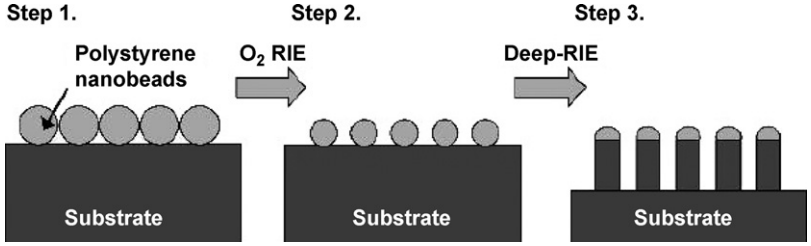

Fig. 7. Schematic illustration of fabricating a nanopillar array by RIE based on the colloidal monolayer mask. Step 1: self-organizing PS colloidal monolayer on the Si substrate. Step 2: decreasing the PS sphere size by oxygen plasma etching. Step 3: fabricating the nanopillar array on the substrate by deep RIE.
Reprinted with permission from Ref. [89]. Copyright 2006 Institute of Physics.

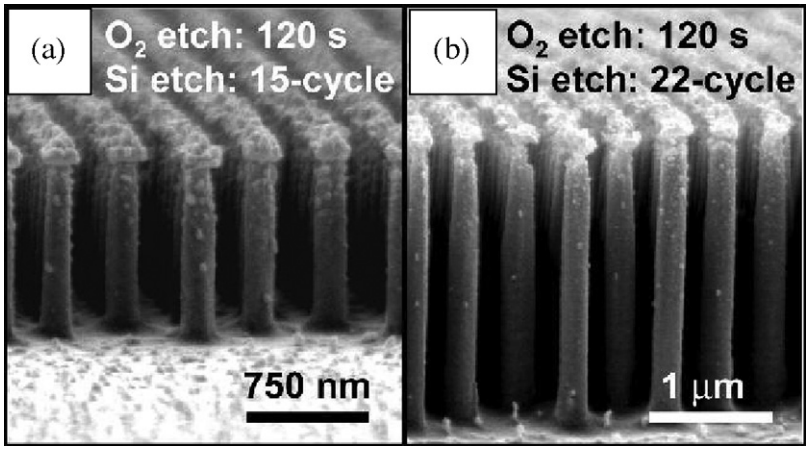

Fig. 8. SEM image of nanopillar arrays fabricated based on a colloidal monolayer Si wafer surface pre-etched with oxygen RIE for 120 s, followed by (a) 15 or (b) 22 cycles of Si etching.
Reprinted with permission from Ref. [89]. Copyright 2006 Institute of Physics.

2.4. Nanorod or nanopillar arrays based on RIE or inductively coupled plasma (ICP) etching

With the direct use of the colloidal monolayer as a mask, a periodic nanopillar or nanorod array can be fabricated on the substrate by RIE [89–91] or ICP [92,93], like conventional top-down techniques. Besides nanopillar arrays, hollow nanopillar arrays have also been created by further treatment of solid nanopillar arrays.

Cheung et al. prepared a PS colloidal monolayer on an Si substrate. The PS sphere size in the colloidal array was tailored by oxygen plasma etching, and an Si nanopillar array was obtained by deep RIE using the ìBoschî process. The fabrication process is depicted in Fig. 7 [89]. The diameter and the length of the nanopillar can be easily tuned by pristine PS sphere size, PS sphere size after tailoring by oxygen plasma etching, and deep RIE time (circle numbers of the Si etching process). The periodicity of the nanopillar arrays can be controlled by colloidal monolayers with different monodisperse sphere sizes. For instance, when the cycles of the etching process were increased from 15 to 22, the aspect ratio of the nanopillar increased markedly (Fig. 8) [89].

Jiang and co-workers developed an interesting technique to prepare an hncp silica colloidal monolayer directly on an Si wafer, combining spin-coating and rapid photopolymerization [90]. The hncp silica colloidal monolayer formed after removal of the polymer among the spheres by oxygen plasma etching, which was used as a mask during the chlorine RIE process. An Si nanopillar array was finally obtained after dissolving the silica sphere in low-concentration HF. Additionally, Choi and Kim et al. created GaN nanorod arrays using colloidal monolayers as masks by inductively coupled plasma (ICP) [92,93].

Utilizing the colloidal monolayer as a mask, a hollow nanopillar array can also be synthesized. For example, Yang and co-workers fabricated a 2D hollow nanopillar array using an SiO_2 nanosphere array by combining a colloidal monolayer mask with RIE on a polymeric film, subsequent sputter deposition of metal on the polymer pillar, and removal of the polymer pillars [94]. First they fabricated ordered silica spheres by spin-coating through self-assembly on PSs film on substrates. The space between the silica sphere monolayer and the PS film was filled with PVA by spin-casting an aqueous PVA solution. A mixture of CF_4 and O_2 RIE was then applied for opening the windows between the silica spheres, and O_2 RIE was used for creating the PS nanopillar array. The rough polymeric layer was completely removed by O_2 RIE process and a polymeric nanopillar array formed under the silica sphere monolayer. Hollow nanopillar arrays of gold and molybdenum nanotube arrays were created on the substrates after sputtering deposition on the nanopillar walls and then removal of the SiO_2 nanosphere on the top as well as the polymeric nanopillar at the bottom. With this approach, the morphologies and sizes of the nanopillars were controlled by simply adjusting the polymer film thickness and the RIE and metal-sputtering conditions.

3. Multiple-step strategies based on colloidal monolayer

Nanoparticle arrays, nanoplate arrays, and nanopore arrays can be easily obtained by the colloidal monolayer template. These periodic arrays can serve as additional masks, patterned catalysis, and patterned substrates to grow periodic 1D nanostructured arrays, including nanowire, nanorod, and nanotube arrays by etching, CVD, electrodeposition, oblique deposition or GLAD, and molecular beam epitaxy (MBE).

3.1. 1D nanostructured arrays based on nanoparticle patterns

Periodic nanoparticle patterns can be synthesized on substrates after evaporation or sputtering deposition of materials on the colloidal monolayer with hexagonal closed packed alignment and subsequent removal of the masks. The elements can be deposited through the interstices among colloidal spheres; hence, such nanoparticle patterns display with a hexagonal arrangement with P6mm symmetry and triangular cross-section. These nanoparticle patterns can be used as masks for further RIE, as patterned catalysts for CVD or MBE growth, or as patterned substrates for sputtering. Periodic nanorod, nanotube, or nanopillar arrays can be grown on the substrates.

3.1.1. Masks for reactive ion etching (RIE)

The periodic nanoparticle patterns obtained by a colloidal monolayer can be further used as masks of RIE for preparing 1D nanostructured arrays [95–99]. Chen and co-workers prepared large-scale, well-ordered periodic nanopillar arrays based on a combination of the colloidal monolayer template method and etching [95–97]. They created periodic Al nanoparticle patterns using the colloidal monolayer as a mask by vapor deposition and then, taking these Al nanoparticle patterns as second masks, prepared Si nanopillar arrays on an Si wafer by RIE using a mixture of CHF_3 and O_2 (Fig. 9) [95]. The size, shape, and height of the nanopillar in the periodic arrays can be well-controlled by fine-tuning the etching recipes (e.g., a flux of CHF_3, O_2 and the total pressure of these two kinds of gases) [95]. They also used Cr nanoparticle

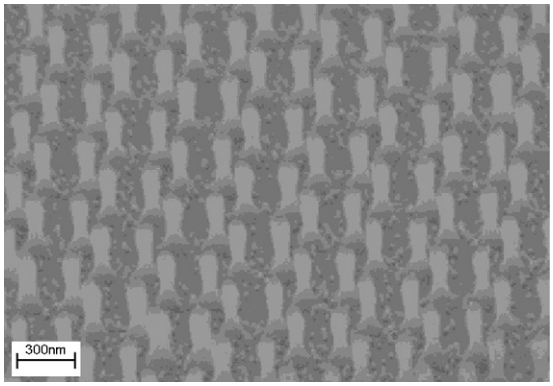

Fig. 9. Periodic Si nanopillar array produced by RIE using Au nanoparticle arrays as the mask.
Reprinted with permission from Ref. [95]. Copyright 2003 American Chemical Society.

patterns obtained by the colloidal monolayer as masks and fabricated Si nanopillar arrays by RIE. Si nanopillar arrays obtained after removing the Cr nanoparticle masks by a chromium etchant were oxidized in an oven that had been purged with oxygen. Nanopillar arrays with sub-10 nm resolution were obtained by removing the oxide layer in an oxide etchant (a BOE solution) [96]. Such high-resolution periodic nanopillar arrays can be used to produce nanoparticles via printing lithography (e.g., nanoimprinting lithography). Simon and co-workers prepared Cr nanoparticle patterns by plasma-assisted physical vapor deposition, using colloidal monolayer masks, and then used the particle arrays as a second mask to synthesize Si nanopillar arrays by RIE of a CF_4/H_2-plasma, which differs from the technique of Chen et al. [98]. They found that the aspect ratio of the nanopillar increased with increased etching time. The height increased but the width of the nanopillar decreased with prolonged etching time; at the same periodicity, the aspect ratio can be increased by increasing the etching time and the nanoparticle size in the second mask [98].

3.1.2. *Patterned catalysts for chemical vapor deposition*

The nanoparticle patterns templated from the colloidal monolayer are used as masks for producing nanopillar arrays by RIE; they can also be applied as patterned catalysts for growing nanotube or nanowire arrays by CVD, MBE, and chemical beam epitaxy (CBE) [100–117]. For instance, Ren et al. first prepared Ni nanoparticle patterns using the colloidal monolayers as masks by electron beam evaporation deposition and then synthesized large-area periodic arrays of well-aligned carbon nanotubes (CNTs) (Fig. 10a) by hot filament plasma-enhanced chemical vapor deposition (PECVD) using the Ni nanoparticle patterns as catalysts [100–103]. The prepared periodic CNT array can act as a photonic crystal in visible range and may be used in optoelectronics. This technique has the advantage of being scaled up at a much lower cost than conventional lithography (e.g., electron beam lithography) [100–108]. Wang et al. synthesized metal catalyst (e.g., Au) nanoparticle patterns from interstices among colloidal spheres in the colloidal monolayer and grew hexagonally patterned, aligned ZnO nanorod arrays using CVD by vapor-liquid-solid growth on a single-crystal alumina substrate [109–113]. The patterned catalyst template resulted in ZnO nanorods in arrays with uniform shape and length, in vertical alignment on the substrate (Fig. 10b). Xie and co-workers developed another method to prepare Au nanoparticle patterns based on colloidal monolayers and synthesized hexagonal ZnO nanorod arrays [114,115]. They did not template the nanoparticle patterns from the interstices among colloidal spheres, but formed an Au catalyst nanodot under each colloidal sphere by selective wet-etching of Au layer on the substrate. They fabricated a PS colloidal monolayer on

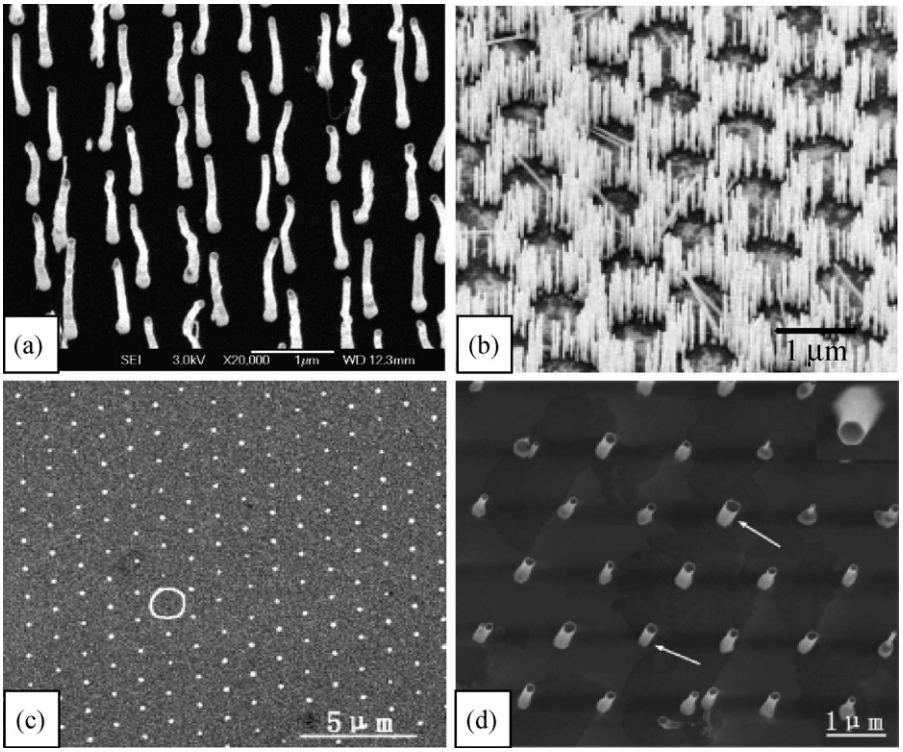

Fig. 10. (a) Periodic CNT arrays grown by PECVD by patterned Ni catalyst nanodot arrays. Reprinted with permission from Ref. [102]. Copyright 2003 American Chemical Society. (b) Aligned ZnO nanorod array grown by patterned Au nanodot catalysts. Reprinted with permission from Ref. [109]. Copyright 2005 Wiley-VCH. (c) Au catalyst particle arrays formed under colloidal monolayer by selective wet etching. (d) ZnO nanorod array produced by the Au catalyst pattern in (c) using CVD. (c and d) Reprinted with permission from Ref. [114]. Copyright 2006 American Chemical Society.

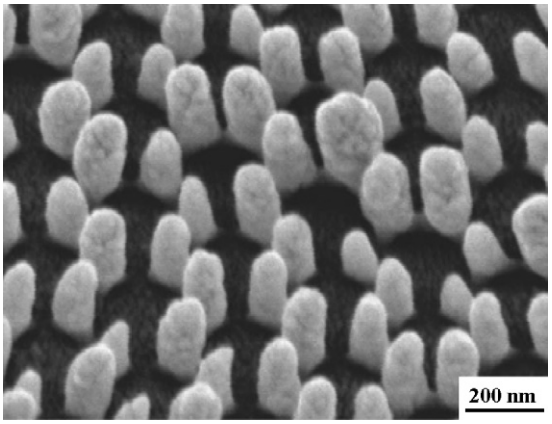

Fig. 11. Ta nanorod arrays by GLAD using a nanodot patterned substrate. Silica colloidal sphere size: 260 nm. Deposition time: 1 h.
Reprinted with permission from Ref. [118]. Copyright 2007 American Institute of Physics.

the octadecanethiol (ODT) modified thin gold layer with a thickness of 1.5–10 nm. The sample was heated at 110 °C for 2 min, and the PS spheres were slightly melted in order to protect the ODT self-assembled monolayer (SAM) under the PS spheres in the subsequent oxygen plasma etching. After plasma etching and removal of PS spheres, Au nanodots were obtained under the PS sphere in the place covered with ODT SAM, and the place uncovered with the ODT SAM (ODT lost by plasma etching) was removed by wet etching with etchants. Thus, Au nanodot patterns were obtained and ZnO nanorod arrays were further prepared for use as patterned catalysts by CVD (Fig. 10c and d) [114,115].

Fuhrmann et al. grew periodic vertically aligned Si nanowire arrays by MBE using pre-formed patterns of gold droplets on Si(1 1 1) substrates based on the colloidal monolayer templates [116]. They removed the native oxide layer by thermal evaporation at 810 °C for 10 min after the gold nanodots templated. Heating at this temperature also transformed the gold nanodots from triangles to hemispheres; however, the arrangement of the gold nanodots remained stable because of the relatively low temperature. The removal of the oxide layer guaranteed further epitaxial growth of Si nanowires. Periodic Si nanowire arrays were grown on the Si substrate at a flux rate of 0.5 Å/s, keeping the substrate at 525 °C or 570 °C by MBE under patterned gold nanodots. Radhakrishnan et al. prepared periodic undoped InP nanowire arrays on Si(1 1 1) using a similar gold nanopattern by CBE [117].

These patterned ZnO, Si, InP, and C nanorod/nanowire/nanotube arrays have many applications such as sensor arrays, nanogenerators, optoelectronic devices, piezoelectric antenna arrays, and interconnects.

3.1.3. Patterned substrate for sputtering

Nanoparticle patterns templated from a colloidal monolayer can be used as a patterned substrate to synthesize nanorod arrays by GLAD, owing to the shadow effect [118,119]. Gall and co-workers prepared Cr nanodot patterns by electron beam evaporation through the quasi-triangular interstices of neighboring spheres in silica colloidal monolayers. Deposition onto this nanodot patterned substrate was performed in an ultrahigh vacuum dc magnetron sputter deposition system with a polar deposition angle of 84° by GLAD. After suitable deposition time, periodic nanorod arrays formed on the patterned substrates (Fig. 11). Nanorod size fluctuation becomes serious in the growth process, due to intercolumnar growth competition; however, the height-to-width ratio of the nanorod remains constant. This result indicates that morphologies of nanorod arrays are determined mainly by geometric shadowing and are independent of the surface diffusion length scale.

3.2. Confined growth of 1D nanostructures based on nanopore patterns

It is quite easy to fabricate periodic nanopore patterns based on the colloidal monolayer templates by sol–gel/solution deposition or electrodeposition after removing the templates. Such nanopore patterns can be further used as templates to grow 1D nanostructures by solution methods and CVD [82–84,120–124].

For instance, Qi et al. prepared periodic silica pore patterns by sol–gel dipping deposition using the PS colloidal template on zinc foil, and successfully grew a ZnO nanorod array on this patterned zinc foil by applying a mixture of $Zn(NO_3)_2$ as well as HMTA as the reacting agent in aqueous solution (Fig. 12) [82–84]. Leu et al. used the colloidal monolayer as the template to prepare a nickel pore pattern by electrodeposition, and synthesized ZnO nanorod arrays on such hexagonally aligned pore patterns by restricting nickel membranes on the Si substrate [120]. They demonstrated that these arrays possessed a field emission property dependent on the density of the ZnO nanorods. Meng and co-workers prepared TiO_2 pore patterns on the Si substrate with Au coating by a colloidal monolayer, and then the SiO_2 restrictedly grew from the pore by CVD using the Au layer as a catalyst [121]. Tai et al. created Mo nanopore arrays by sputtering on the Si substrate, using a colloidal monolayer mask [122,123]. After removal of the colloidal mask, a Co/Ti catalyst layer coating was deposited on the Mo nanopore patterns. The patterned CNT arrays were finally synthesized by rapid-heating CVD at 450 °C, using the Co/Ti layer as a catalyst. The Mo poisoned the catalyst and prevented CNT growth where deposited, resulting in a periodic CNT pattern [122].

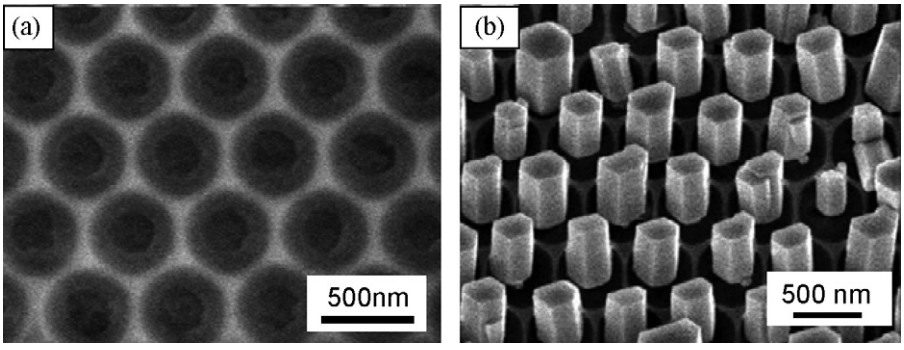

Fig. 12. (a) Silica pore patterns templated from a PS colloidal monolayer on zinc foil. (b) Periodic ZnO nanopillar arrays grown in silica pore arrays.
Reprinted with permission from Ref. [82]. Copyright 2009 American Chemical Society.

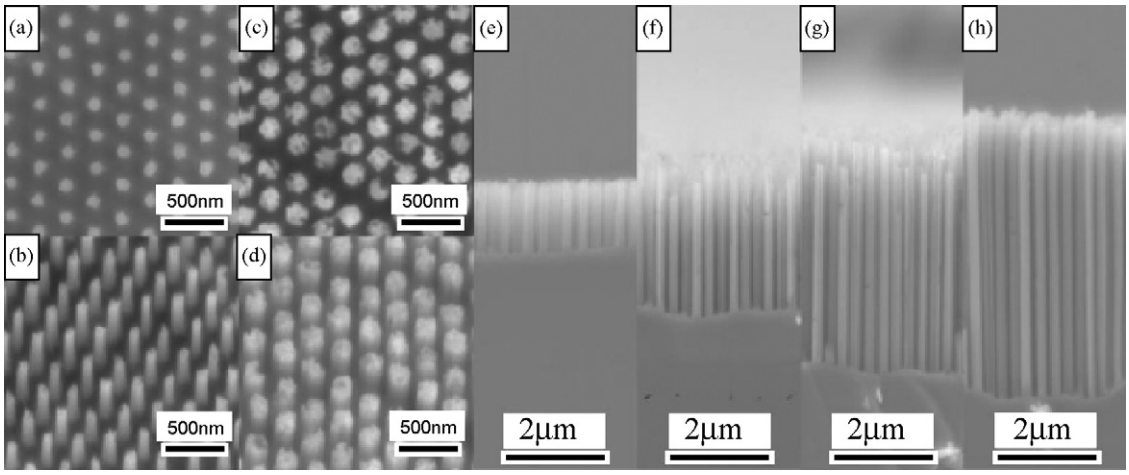

Fig. 13. SEM images where a PS sphere with a pristine size of 260 nm was used. (a and c) Plane view. (b and d) Tilted view at 15°. The sphere sizes were decreased to (a and b) 100 nm and (c and d) 180 nm. Cross-sectional images after etching for (e) 4 min, (f) 8 min, (g) 12 min, (h) 16 min.
Reprinted with permission from Ref. [125]. Copyright 2007 Wiley-VCH.

3.3. Catalytic chemical etching based on noble metal network nanoskeletons

Noble metal network nanoskeletons in the pore patterns can be synthesized using an hncp colloidal monolayer template by physical deposition of noble metal after removal of the template. These skeletons can be used as catalysts to chemically etch the substrate, and nanorod arrays form where these catalysts are uncovered [125,126]. Zhu and co-workers developed a strategy to fabricate Si nanowire arrays based on the colloidal monolayer and following catalytic chemical etching [125]. Briefly, the hncp colloidal monolayer was achieved by RIE of the hcp monolayer on the Si substrate. A catalyst layer of silver film was deposited by thermal evaporation on the hncp colloidal monolayer and an Ag film with a hexagonal network under PS but on the silicon substrate. This Ag film could serve as a catalyst for chemical etching of the Si using a mixture of deionized water, HF and H_2O_2. The Si under the catalyst would be etched away, and nanowires would form under the hncp PS spheres. Finally, the Si nanowire array was obtained after removal of the PS sphere and Ag catalyst by selective chemical dissolution. With this method, the nanowire diameter can be controlled by colloidal nanosphere size after RIE, the nanowire number density can be tuned by pristine colloidal monolayers with various periodicities, and the nanowire length can easily be increased by increasing the chemical etching time (Fig. 13).

3.4. 1D nanostructured arrays based on periodic nanodisk patterns

Periodic nanodisk patterns can be fabricated on a substrate by two-step replication based on the colloidal monolayer templates. The periodic pore patterns are prepared using the colloidal monolayer as the first templates; then they are applied to synthesize the nanodisk patterns as second sacrificial templates. These nanodisks can be used for masks to prepare nanorod arrays on substrates by RIE or electrochemical etching. Goedel and co-workers fabricated polymer pore arrays on the Si wafer by polymerization, using colloidal templates, and then deposited gold on the pore patterns on the supporting substrate by vapor deposition [127]. After removal of the pore-patterned polymer, the gold nanodisk patterns remained on the substrate, and Si pillar arrays with a large area were obtained by deep RIE, using them as masks (Fig. 14). Jiang fabricated a pore-patterned polymer layer using silica hncp colloidal monolayer templates, and nickel nanodisk patterns were further fabricated using the porous polymer layer as second masks by sputtering deposition. The Si nanopillar arrays were finally achieved by RIE with the nickel nanodisk masks [128]. In addition to the two-step replication, nanodisk arrays can be prepared directly using colloidal monolayers as masks. Desired materials are coated on the bare substrate, and then colloidal monolayers are fabricated on the substrate with the desired material coating; periodic nanodisk patterns are obtained by RIE using the colloidal monolayer

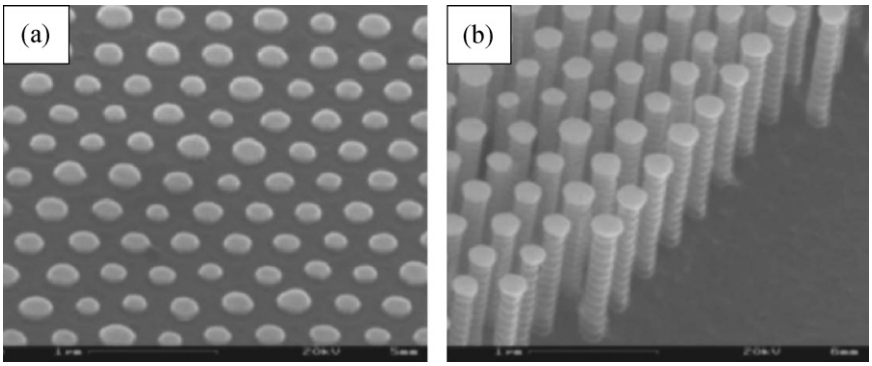

Fig. 14. (a) Au nanodisk etch mask formed at the sites of the former pore array mask. (b) Si nanopillars with gold dots on top produced by RIE. Scale bar: 1 μm.
Reprinted with permission from Ref. [127]. Copyright 2007 American Institute of Physics.

as a mask after its removal. For instance, Yang and co-workers prepared nitride nanodisks under colloidal spheres by RIE on a substrate using colloidal spheres as masks; Si nanopillar arrays were then fabricated using photo-assisted electrochemical etching with the help of Cr/Cu films on the backside of an Si wafer [129].

4. Applications and devices

Based on one-step or multiple-step strategies using colloidal monolayer templates or masks, the morphologies and structural parameters (sizes and spacings of a 1D nanostructured unit) of periodic 1D nanostructured arrays (e.g., nanorod, nanowire, nanopillar, and nanotube arrays) can be easily tuned by periodicities of colloidal monolayers, experimental conditions such as deposition or etching time, background gas pressure, or recipe of electrolytes. Some properties, such as the surface wettability, field emission, light-emission, and photonic bandgaps, are closely morphology- and structural parameter-dependent. These properties can be readily optimized by tuning morphologies and parameters of the periodic arrays. Their investigations supply useful theoretic foundations and are highly valuable for designing micro/nanodevices based on these 1D nanostructured arrays.

4.1. Self-cleaning films

A self-cleaning surface is usually defined as a surface that has the ability to remove dirt or contaminants that are on it when water droplets slide along the surface. Self-cleaning is closely related to surface wettability [130–135]. The self-cleaning effect is normally attributed to superhydrophobicity (water contact angle (CA) exceeding 150° and sliding angle (SA) less than 10°) or superhydrophilicity (water CA less than 10°) of the surface. For superhydrophobicity with a self-cleaning effect, contaminants adhere to the water droplet surface and are removed after the water droplet slides off the solid surface with a small tilted angle, due to large water CA and low surface free energy. For superhydrophilic surfaces, contaminants can easily be swept away by adding water droplets on them, due to very low water CA. Wettability can be enhanced by increasing surface roughness, according to Wenzel's equation [136]:

$$\cos\theta_r = r\cos\theta \quad (1)$$

where r is the roughness factor, defined as the ratio of total surface area to projected area on the horizontal plane; θ_r is the CA of film with a rough surface; and θ is the CA of film with a smooth surface. Obviously, increased roughness can enhance the hydrophobicity and/or hydrophilicity of hydrophobic and/or hydrophilic surfaces.

The 1D nanostructured periodic arrays based on colloidal monolayers are actually rough films at the nanoscale level. It is expected that such 1D nanostructured arrays could induce surface superhydrophilicity or superhydrophobicity with a self-cleaning effect, due to their high roughness.

Amorphous, porous 1D TiO_2 nanorod arrays were prepared by combining PLD using colloidal monolayers (Fig. 3) [72]. These arrays exhibited strong superhydrophilicity. When a small water droplet was dropped on a nanorod array, the droplet spread out rapidly on the surface and displayed a water CA of 0° in a 0.225 s (Fig. 15). Additionally, this nanorod film exhibited superoleophilicity when a small oil droplet was placed on the nanorod surface and the oil CA became 0° in 0.5 s. These results suggest that this amorphous 1D nanorod array had superamphiphilicity with 0° of both water CA and oil CA.

A TiO_2 film with superamphiphilicity can generally be obtained by UV irradiation, due to hydroxyl ions generated by oxygen defects or dangling bonds on its surface, induced by photochemical processes [137]. However, in this study, the TiO_2 nanorod array film possessed superamphiphilicity without further UV irradiation. The ions (e.g., Ti^{4+}, and O^{2-}) and electrons are released into the PLD chamber and some oxygen species are lost in the vacuum environment in PLD after a TiO_2 target absorbs energy from laser irradiation by exceeding its threshold. Oxygen vacancies are produced in the deposited TiO_2 during PLD, converting relevant Ti^{4+} sites to Ti^{3+}

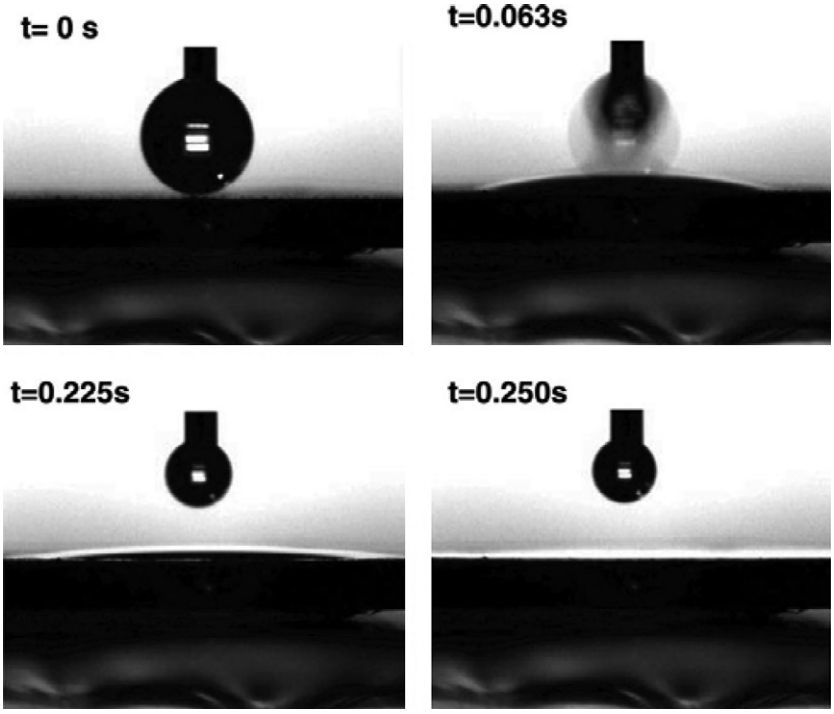

Fig. 15. Time course of water-contacting behavior on the hcp 1D amorphous TiO_2 nanorod array film. Reprinted with permission from Ref. [72]. Copyright 2008 American Chemical Society.

sites that are favorable for dissociative water adsorption. Therefore, these defect sites microscopically form hydrophilic domains on the TiO_2 surface. However, the other parts surrounding the hydrophilic domain remain oleophilic on the surface. A composite TiO_2 surface having hydrophilic and oleophilic domains on a microscopically distinguishable scale demonstrates macroscopic amphiphilicity on the TiO_2 surface [137]. Additionally, a TiO_2 nanoparticle film prepared by PLD without a PS colloidal monolayer exhibited a water CA of 15° and an oil CA of 27°. The roughness of the 1D hcp TiO_2 nanorod array film was greatly increased compared with that of the nanoparticle TiO_2 film produced by PLD without using a colloidal monolayer. According to Wenzel's equation, wettability is enhanced from amphiphilicity to superamphiphilicity. Therefore, the superamphiphilicity of the amorphous 1D nanorod array originates from the combination of the amphiphilicity produced by PLD and the special rough structures of hcp hierarchical nanorod arrays.

More importantly, this amorphous TiO_2 nanorod array demonstrated very good photocatalytic activity for organic molecular degradation (e.g., effective decomposition of stearic acid under UV illumination) [72]. Compared with other TiO_2 films (e.g., an amorphous TiO_2 film produced by PLD without using a colloidal monolayer and an anatase TiO_2 nanorod array), the hcp amorphous 1D TiO_2 nanorod array on the colloidal monolayer demonstrated the best performance for degradation of organic materials, which is attributed to its porous structures and a much higher specific surface area than that of an anatase nanorod array. Besides the higher specific surface area, special hierarchical structures composed of radiation-shaped nanobranches emanating from a center point on the PS sphere of a periodic structured nanorod array of amorphous TiO_2 can enhance photocatalytic activity, compared to an amorphous TiO_2 thin film produced by PLD without using a colloidal monolayer.

A combination of superamphiphilicity and photocatalytic activity can yield a self-cleaning surface. For instance, an oily liquid contaminant spreads out on a surface due to superoleophilicity, which is helpful in improving the photocatalytic efficiency under light illumination. An organic contaminant including oil gradually degrades under sunlight irradiation (sunlight contains some UV light). The self-cleaning effect can be realized after washing away contamination from the superhydrophilic surface.

Additionally, superhydrophobic surfaces with large water CA and small SA have a self-cleaning effect. For superhydrophobic film, the surface should be sufficiently rough and have a chemical coating with low free-energy materials in order to trap the air on the rough surface. In this case, the area fraction of a water droplet in contact with the sample surface is very small, which helps obtain a small SA [130–135]. Periodic 1D nanostructured arrays based on colloidal templates provide surfaces with regularly ordered and well-defined roughness. They may lead to enhancement from hydrophobicity to superhydrophobicity on the surface after modification with low free-energy materials [138–140]. For instance, Jiang and co-workers prepared periodic Si nanopillar arrays using an hncp silica colloidal monolayer mask by chlorine RIE after removing the colloidal sphere mask [138]. With this method, nanopillar depth increases with increased etching time. The increasing aspect ratio can significantly enhance the hydrophobicity of the surface, due to the high fraction of air trapped in such a rough surface composed of nanopillars after being functionalized with fluorosilane through the well-established silane coupling reaction. An Si nanopillar array templated from the colloidal monolayer composed of 380 nm spheres demonstrated superhydrophobicity with a self-cleaning effect (water CA of 172°) after 60 min RIE [138]. Yang and co-workers synthesized Si hollow-tip arrays with a high aspect ratio using metal catalytic wet-etching Si followed by short-time RIE based on the colloidal monolayer templates [139]. They also discovered that such Si hollow-tip arrays effectively trapped air on the array surface after modification with fluorosilane, and hence displayed strong superhydrophobicity with water CA of 162° and SA of 2°.

4.2. Field emitters

Field-emission (FE) properties have recently attracted much attention as a result of commercial interest in flat-panel displays and other microelectronic devices [141]. Besides CNTs, semiconductors have attracted great interest as field emitters because of their mechanical stability, low work function, and superior electrical and thermal conductivities [142]. FE properties are usually decided by the nature of the cathode materials as well as their geometry and size. By effectively designing the geometry and size of the cathode (e.g., to introduce nanostructures on it), good FE characteristics (such as faster turn-on time, compactness, and sustainability during the field emission) have been achieved, compared to those of conventional bulky material forms. More importantly, researchers have found that cathodes composed of periodic regular arrays on the surface are very helpful for producing a low operating voltage and a stable current because of the elimination of the shield effect on densely packed 1D nanostructured arrays in field emission.

Periodic TiO_2 nanorod arrays with hncp arrangement can be synthesized by combining a colloidal monolayer template with PLD, followed by annealing in ambient air [76]. Thus, the periodicity of the nanorods can be easily tuned by changing the colloidal sphere size in the colloidal monolayer template. The distance between neighboring nanorods can be controlled by varying the background gas pressure during PLD if periodicity is fixed for a nanorod array. The easily tunable periodicity and distance between neighboring nanorods are very useful for investigating and optimizing their FE performance [76].

A periodic hncp TiO_2 nanorod array was fabricated by PLD using a colloidal monolayer template with 350 nm PS spheres at 6.7 Pa O_2 for 60 min and subsequent annealing at 650 °C for 2 h in air (Fig. 16). It demonstrated a low turn-on field of 5.6 V μm^{-1} (here, defined as the value of the electric field when the emission current density is 4.5 nA cm^{-2}) according to the FE current density–applied electric field curve (J–E) at a working distance of 60 μm from the anode to the nanorod array serving as the cathode. This FE current–voltage characteristics can be expressed by a simplified Fowler–Nordheim (FN) equation and a field-enhancement factor, β can be defined as $B\phi^{3/2}/\kappa$ according to the FN equation (here, ϕ: the work function of the cathode material; κ: the slope in the FN plot) [143]. This hncp TiO_2 nanorod array showed a field-enhancement factor β of 8.38×10^2. However, a TiO_2 nanorod array with top aggregation for several neighboring nanorods caused by longer deposition displayed a much higher turn-on field of 15.8 V μm^{-1} and lower field-enhancement factor β of 3.34×10^2. This result indicates that the good FE properties of a periodic TiO_2 hncp nanorod array are mainly attributable to the aligned and periodic hncp nanorod morphology.

The periodicity of the hncp nanorod array was increased from 350 nm to 750 nm and 1 μm by choosing colloidal monolayers with different PS sphere sizes during PLD at the same background gas pressure as before and followed by the same annealing. The field-enhancement factor decreased with increasing periodicity of the hncp nanorod array (Fig. 17a), mainly because of a decreasing number density of nanorods with an increase in hncp array periodicity. When the periodicity of the hncp nanorod array was increased from 350 to 750 nm, the turn-on field increased from 5.6 to 13.0 V μm^{-1}. When periodicity further increased to 1 μm, the turn-on field remained at 13.0 V μm^{-1}. It is evident that the hncp nanorod array with the smallest periodicity of 350 nm exhibited the best FE properties in this investigation.

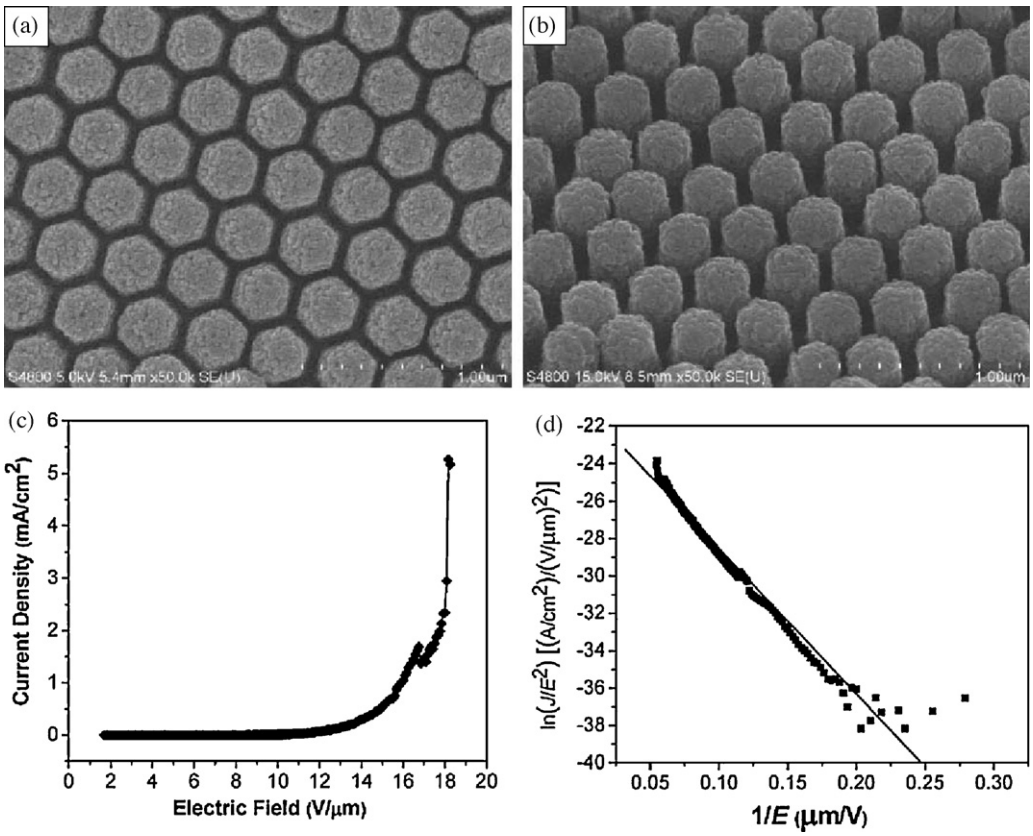

Fig. 16. Periodic hncp nanorod array produced by PLD using a colloidal monolayer template with 350 nm PS spheres in O_2 at a pressure of 6.7 Pa for 60 min and subsequent annealing in air. (a) Top-view. (b) Tilted view with an angle of 45°. (c) FE current density–electric field (J–E) curves measured for an hncp TiO_2 nanorod array at an anode–cathode distance of 60 μm. (d) Corresponding Fowler–Nordheim (FN) plot.
Reprinted with permission from Ref. [76]. Copyright 2009 Wiley-VCH.

The distance between neighboring nanorods can be tuned by changing the background gas pressure during PLD if periodicity is fixed at 350 nm for a nanorod array (Fig. 4). With increased distance, the field-enhancement factor increased and the turn-on field decreased (Fig. 17a). The sample with a small nanorod distance of 20 nm exhibited a relatively low field-enhancement factor of 5.04×10^2 and a high turn-on field of $9.7\,V\,\mu m^{-1}$. When the nanorod distance increased to 50 nm, the FE properties indicated enhanced performance with a high field-enhancement factor of 8.38×10^2 and a low turn-on field of $5.6\,V\,\mu m^{-1}$. When the nanorod distance further increased to 110 nm, the best FE properties with a field-enhancement factor of 9.39×10^2 and a turn-on field of $5.3\,V\,\mu m^{-1}$ were obtained (Fig. 17b). These results suggest that optimized FE properties can be achieved by increasing the nanorod distance and controlling the experimental parameters. The increased field-enhancement factor β with increased nanorod distance can easily be understood as follows if the periodicity of the hncp nanorod array is fixed. The field enhancement factor β is generally related to the geometry of an emitter and can be expressed as $\beta \propto h/r$, where h is the height and r is the curvature radius of an

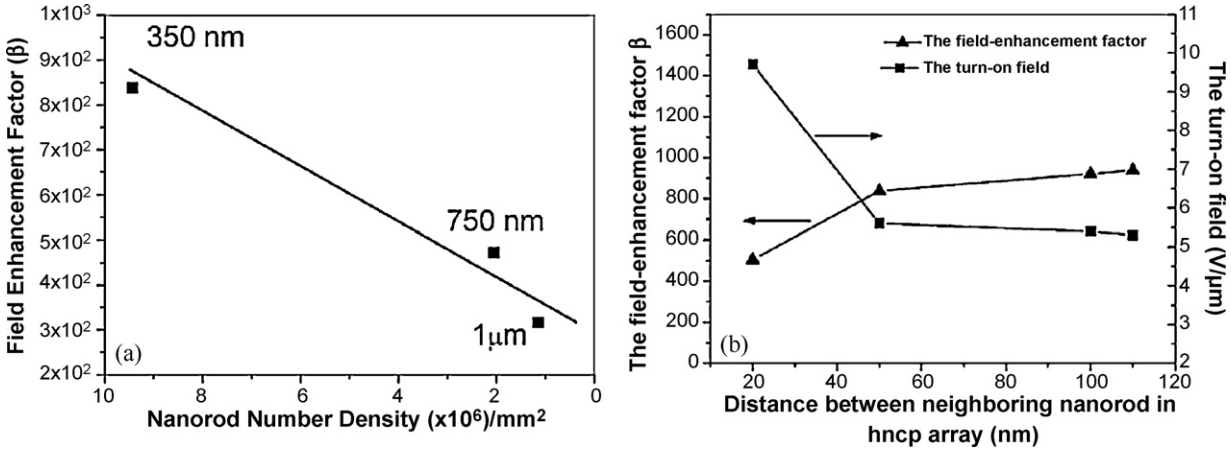

Fig. 17. (a) Field-enhancement factor β changing with increasing periodicity of an hncp nanorod array. (b) Change in field-enhancement factor and turn-on field with varying neighboring nanorod distances in an hncp array.
Reprinted with permission from Ref. [76]. Copyright 2009 Wiley-VCH.

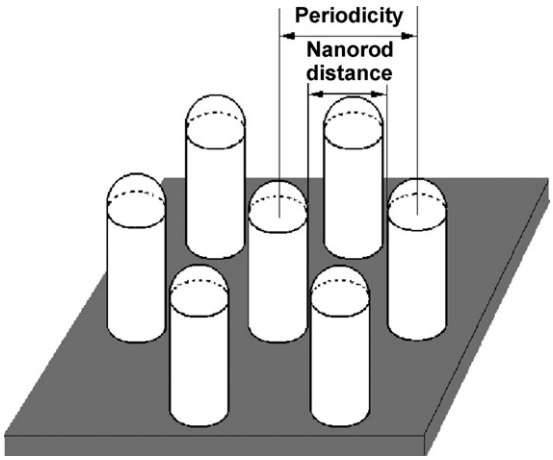

Fig. 18. Schematic illustration of a defined nanorod distance in a periodic hncp nanorod array.
Reprinted with permission from Ref. [76]. Copyright 2009 Wiley-VCH.

emitting center. With an increase in nanorod distance, the effective diameter of an individual nanorod and the curvature radius r decrease (Fig. 18), resulting in an increase of β according to the above relationship.

4.3. Photonic crystals

Photons are widely used as information carriers, due to the large capacity of bandwidth optical fibers and effective transportation for a long distance. However electronic processing of photonic signals is currently required at each circuit node by optical fiber transporting. Therefore, the photons are expected to pass directly through each node. Direct optical interconnects (e.g., photonic crystals or photonic band gap (PBG) materials) have this effect to localize and guide light. Photonic crystals are usually defined as periodic dielectric structures with an index of refraction periodicity of the order of the wavelength of light being localized [144]. The performance of the photonic crystal is completely determined by the index of refraction periodicity, but not optical absorption or emission of materials. The periodic nanostructured array is a kind of photonic crystal, according to its features, and is able to control light from UV to visible range.

Ren and co-workers prepared large-scale periodic arrays of aligned CNTs using Ni nanodot catalysts made by colloidal monolayer templates through PECVD (Fig. 10a) [102]. This periodic CNT array appeared colorful because of the strong diffraction of visible light (Fig. 19a–c). The CNT honeycomb array is a hexagonal two-dimensional (2D) Bravais lattice with a basis and its light diffraction can be explained by related theory. From the diffraction pattern of different frequencies, the diffraction pattern obtained from the CNT honeycomb lattice should be a triangular lattice. This highly rotationally symmetric pattern reveals a CNT array that is circularly symmetric in the plane, and a small hexatic distortion of the diffraction pattern reflects that CNTs in the array are not perfectly straight (Fig. 19d). Such a CNT array can act as 2D PBG crystals, due to the different dielectric constants from the environment, which not only act on propagating photons by Bragg scattering but are also in complete analogy with the electron propagation in atomic crystals, finally leading to the opening of energy (frequency) gaps at the Bragg reflection points. The existence of such gaps at all propagation directions of the photon results in an absolute gap in the photonic spectrum, further leading to a total reflection of light in this frequency band for the photonic crystal.

However, the periodic 1D CNT or ZnO nanorod arrays based on colloidal template techniques have the disadvantages of a large percentage of air space and a vanishing photonic bandgap in applications of photonic crystals. Wang et al. further improved 1D nanostructured arrays in the photonic application by coating TiO_2 on the nanorod arrays [109]. They first prepared a ZnO nanorod array using a gold nanodot pattern as a catalyst templating from a colloidal monolayer. The amorphous TiO_2 layer was then uniformly coated on the ZnO nanorod pattern by low-temperature atomic layer deposition (ALD). They obtained a continuous dielectric film of TiO_2-coated ZnO nanorod array with a periodic air-hole array (Fig. 20). The achieved structure has the advantage of high refrac-

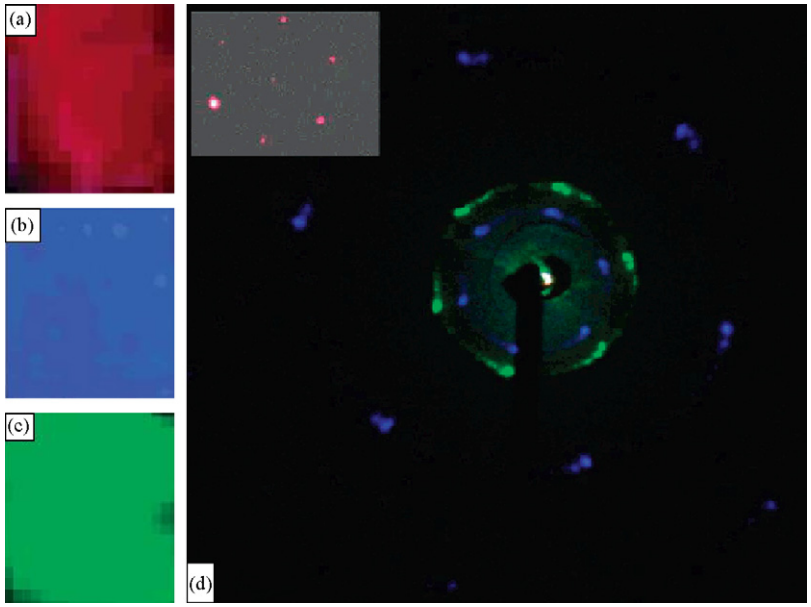

Fig. 19. The CNT array took on different colors when the white light was perpendicular to the sample. (a) Red observed from 51.8°, (b) blue observed from 31.7° and (c) green color observed from 40.3°. (d) Light-diffraction pattern at different frequencies produced by the CNT arrays with $a = 1\ \mu m$. The diffraction pattern was obtained by green (560 nm) and blue (454 nm) laser light perpendicular to the plane of the lattice. The inset is the diffraction pattern for a red light (680 nm), obtained at an incidence of 45°.
Reprinted with permission from Ref. [102]. Copyright 2003 American Chemical Society.

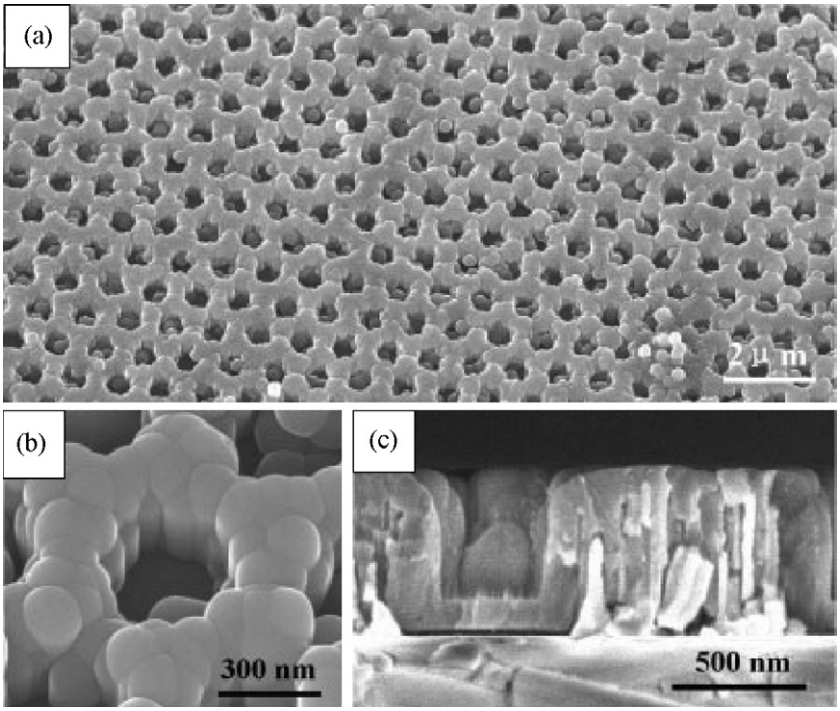

Fig. 20. TiO_2/ZnO quasi-2D photonic crystal structure. (a) Low-magnification SEM image. (b) Feature image depicting a single air hole in a TiO_2 coated ZnO nanorod. (c) Cross-section of a periodic ZnO nanorod with a TiO_2 coating array.
Reprinted with permission from Ref. [109]. Copyright 2005 Wiley-VCH.

tive index contrast and is very similar to the 2D photonic crystal slab; therefore, it can be used as a photonic crystal. They observed a reflection peak at 2670 nm from this structure, which is close to the theoretically predicted bandgap region from 2243 to 2440 nm. The mismatch of ~12% between the observed value and the theoretical value can be attributed to several assumptions and simplifications in the theoretical calculation [109].

Chen and co-workers fabricated a periodic ZnO nanorod network array by the aqueous chemical method using a colloidal monolayer template. This ZnO nanostructured array also exhibited a photonic crystal band gap centered at 437 nm, which is an excellent match with the calculated value [145].

4.4. Antireflection coatings

For photovoltaic devices, to achieve a large improvement of the conversion efficiencies of sunlight, the full solar spectrum should be absorbed as much as possible in the first step. Unfortunately, a large percentage of incident light is reflected back from the surface of the materials of solar cells, due to their high refractive indexes (for instance, 30% reflection for crystalline Si and GaAs, and 40% reflection for GaSb). Traditional anti-reflective coatings (ARCs) are usually prepared by vacuum deposition of multilayer dielectric films; however, they have the disadvantages of high cost and poor thermal stability [146]. Inspired by the corneas of moths, which greatly reduce reflection by creating the reflective index gradient caused by hncp subwavelength conical nipples [147,148], promising techniques of introducing periodic nanostructured arrays or gratings have been developed to prepare an ARC [149–152]. For example, Jiang and co-workers prepared an Si hncp nanopillar array by applying an hncp silica colloidal monolayer as a mask by chlorine RIE after removing the colloidal sphere mask [149]. The prepared hncp Si nanopillar arrays exhibited normal-incidence reflection that was greatly reduced to less than 2.5% from more than 30% for a flat Si wafer. This nanopillar array ARC also exhibited excellent broadband anti-reflection properties, even better than the crystalline Si solar cell with a commercial SiN_x ARC (Fig. 21). In addition to Si nanopillar arrays, they prepared similar GaAs and GaSb ARCs, and achieved broadband anti-reflection performance due to such bionic structures [151,152].

Other applications (e.g., light emission or light-emitting diode (LED)) based on GaN, InGaN/GaN nanorod arrays obtained by RIE using colloidal templates have also been investigated, due to commercial interest in high-brightness LEDs or solid-state lighting and backlight modules of flat panel displays [153–155].

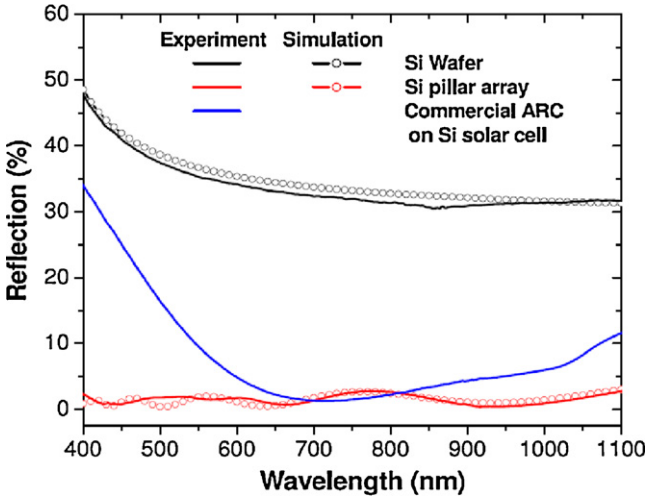

Fig. 21. Experimental and simulated reflective spectra at normal incidence from a flat Si wafer (black), a commercial Si solar cell with SiN_x ARC (blue), and an hncp Si nanopillar array templated from a colloidal monolayer (red).
Reprinted with permission from Ref. [149].

5. Conclusions and outlook

The colloidal monolayer has proven to be an effective, inexpensive, versatile template or mask to create periodic 1D nanostructured arrays with controlled morphologies, sizes, and periodicities. Based on one-step or multiple-step strategies using colloidal monolayer templates or masks, various periodic 1D nanostructured arrays (e.g., nanowire, nanorod, nanopillar, and nanotube arrays) can be synthesized by chemical methods (such as electrodeposition, solution deposition, and wet chemical etching) and physical methods (such as PLD, sputtering, electron-beam deposition, RIE, and CVD). In principle, the morphologies of these 1D nanostructured arrays can be tuned by controlling the experimental conditions (e.g., etching or deposition time, background gas pressure in the vacuum chamber, concentration of precursor solution, electrolyte recipe, and periodicity of the colloidal monolayer). Compared with chemical methods, physical methods are more suitable for preparing high-quality 1D nanostructured arrays with uniform morphologies with uniform morphologies due to their own characters. Morphology- or size-dependent properties (e.g., superamphiphilicity, superhydrophobicity, photocatalytic activity, field emission, photonic bandgap, light emission, and anti-reflection) were investigated, which have important applications in devices, microfluidic devices, field emitters, waveguide based on photonic crystals, light-emitting diodes, and solar cells. Compared to the development of synthesized strategies of 1D nanostructured arrays, morphologies or parameters have not been investigated so much, especially for nanodevices dependent on 1D nanostructured arrays. More nanodevices with improved characteristics based on such 1D nanostructured arrays with different materials are expected, and we believe that more exciting results will be achieved through researchers' endeavors in the near future.

Acknowledgements

This work was financially supported by the Natural Science Foundation of China (Grant Nos. 50831005, 50601026, 10974203) and the Major State Research Program of China, "Fundamental Investigation on Micro-Nano Sensors and Systems based on BNI Fusion" (Grant No. 2006CB300402).

References

[1] Y. Xia, P. Yang, Y. Sun, Y. Wu, B. Mayers, B. Gates, Y. Yin, F. Kim, H. Yan, Adv. Mater. 15 (2003) 353.
[2] Z.L. Wang, ACS Nano 2 (2008) 1987.
[3] J. Hu, T.W. Odom, C.M. Lieber, Acc. Chem. Res. 32 (1999) 435.
[4] C. Xie, Y. Cui, Proc. Natl. Acad. Sci. 107 (2010) 4489.
[5] G.M. Wallraff, W.D. Hinsberg, Chem. Rev. 99 (1999) (1801).
[6] T. Ito, S. Okazaki, Nature 406 (2000) 1027.
[7] H.I. Smith, M.L. Schattenburg, IBM J. Res. Dev. 37 (1993) 319.
[8] J.A. Stroscio, D.M. Eigler, Science 254 (1991) 1319.
[9] G.-Y. Liu, S. Xu, Y. Qian, Acc. Chem. Res. 33 (2000) 457.
[10] R.D. Piner, J. Zhu, F. Xu, S. Hong, C.A. Mirkin, Science 283 (1999) 661.
[11] M. Steinhart, J.H. Wendorff, A. Greiner, R.B. Wehrspohn, K. Nielsch, J. Schilling, J. Choi, U. Gösele, Science 296 (2002) 1997.
[12] M. Steinhart, R.B. Wehrspohn, U. Gösele, J.H. Wendorff, Angew. Chem. Int. Ed. 43 (2004) 1334.
[13] W. Stöber, A. Fink, J. Colloid Interface Sci. 26 (1968) 62.
[14] D. Zou, V. Derlich, K. Gandhi, M. Park, L. Sun, D. Kriz, Y.D. Lee, G. Kim, J.J. Aklonis, R. Salovey, J. Polym. Sci. A: Polym. Chem. 28 (1990) 1909.
[15] R. Arshady, Colloid Polym. Sci. 270 (1992) 717.
[16] R. Micheletto, H. Fukuda, M. Ohtsu, Langmuir 11 (1995) 3333.
[17] N.D. Denkov, O.D. Velev, P.A. Kralchevsky, I.B. Ivanov, H. Yoshimura, K. Nagayama, Nature 361 (1993) 1303.
[18] C.L. Haynes, R.P. van Duyne, J. Phys. Chem. B 105 (2001) 5599.
[19] G.A. Ozin, S.M. Yang, Adv. Funct. Mater. 11 (2001) 95.
[20] P. Jiang, M.J. McFarland, J. Am. Chem. Soc. 126 (2004) 13778.
[21] D. Wang, H. Möhwald, Adv. Mater. 16 (2004) 244.
[22] Y. Li, W.P. Cai, G.T. Duan, F.Q. Sun, B.Q. Cao, F. Lu, Mater. Lett. 59 (2005) 276.
[23] S. Antony, A.S. Dimitrov, K. Nagayama, Langmuir 12 (1996) 1303.
[24] P.A. Kralchevsky, N.D. Denkov, Curr. Opin. Colloid Interface Sci. 6 (2001) 383.
[25] S.H. Im, M.H. Kim, O.O. Park, Chem. Mater. 15 (2003) 1797.
[26] V. Kitaev, G.A. Ozin, Adv. Mater. 15 (2003) 75.
[27] N.D. Denkov, O.D. Velev, P.A. Kralchevsky, I.B. Ivanov, H. Yoshimura, K. Nagayama, Langmuir 8 (1992) 3183.
[28] W.M. Choi, O.O. Park, Nanotechnology 17 (2006) 325.
[29] A.A. Chabanov, Y. Jun, D.J. Norris, Appl. Phys. Lett. 84 (2004) 3573.
[30] L. Meng, H. Wei, A. Nagel, B.J. Wiley, L.E. Scriven, D.J. Norris, Nano Lett. 6 (2006) 2249.
[31] M. Kondo, K. Shinozaki, L. Bergström, N. Mizutani, Langmuir 11 (1995) 394.
[32] A. Kosiorek, W. Kandulski, H. Glaczynska, M. Giersig, Small 1 (2005) 439.
[33] J. Rybczynski, U. Ebels, M. Giersig, Colloids Surf. A: Physicochem. Eng. Aspects 219 (2003) 1.
[34] M. Retsch, Z. Zhou, S. Rivera, U. Jonas, M. Kappl, X.S. Zhao, Q. Li, Macromol. Chem. Phys. 210 (2009) 230.
[35] S.-M. Yang, S.G. Jang, D.-G. Choi, S. Kim, H.K. Yu, Small 2 (2006) 458.
[36] G. Zhang, D. Wang, Chem. Asian J. 4 (2008) 236.
[37] Y. Li, W.P. Cai, G.T. Duan, Chem. Mater. 20 (2008) 615.
[38] H.W. Deckman, J.H. Dunsmuir, Appl. Phys. Lett. 41 (1982) 377.
[39] M.D. Malinsky, K.L. Kelly, G.C. Schatz, R.P. van Duyne, J. Phys. Chem. B 105 (2001) 2343.
[40] F. Sun, W. Cai, Y. Li, G. Duan, W.T. Nichols, C. Liang, N. Koshizaki, Q. Fang, I.W. Boyd, Appl. Phys. B: Lasers Opt. 81 (2005) 765.
[41] F. Burmeister, C. Schäfle, T. Matthes, M. Böhmisch, J. Boneberg, P. Leiderer, Langmuir 13 (1997) 2983.
[42] J. Pacifica, D. Gómez, P. Mulvaney, Adv. Mater. 17 (2005) 415.
[43] B.J.Y. Tan, C.H. Sow, T.S. Koh, K.C. Chin, A.T.S. Wee, C.K. Ong, J. Phys. Chem. B 109 (2005) 11100.
[44] J. Sort, H. Glaczynska, U. Ebels, B. Dieny, M. Miersig, J. Rybczynski, J. Appl. Phys. 95 (2004) 7516.
[45] A.J. Haes, C.L. Haynes, R.P. van Duyne, Mater. Res. Soc. Symp. 636 (2001), D4.8.1.
[46] A.V. Whitney, B.D. Myers, R.P. van Duyne, Nano Lett. 4 (2004) 1507.
[47] Y. Li, W.P. Cai, G.T. Duan, F.Q. Sun, F. Lu, Appl. Phys. A: Mater. Sci. Process. 81 (2005) 269.
[48] Y. Li, W.P. Cai, B.Q. Cao, G.T. Duan, C.C. Li, F.Q. Sun, et al., J. Mater. Chem. 16 (2006) 609.
[49] F.Q. Sun, W.P. Cai, Y. Li, L.C. Jia, F. Lu, Adv. Mater. 17 (2005) 2872.
[50] F.Q. Sun, W.P. Cai, Y. Li, B.Q. Cao, F. Lu, G.T. Duan, C.C. Li, F.Q. Sun, H.B. Zeng, Adv. Mater. 16 (2004) 1116.
[51] B.Q. Cao, W.P. Cai, F.Q. Sun, Y. Li, Y. Lei, L.D. Zhang, Chem. Commun. (2004) 1604.
[52] G.T. Duan, W.P. Cai, Y. Li, Z.G. Li, B.Q. Cao, Y.Y. Luo, J. Phys. Chem. B 110 (2006) 7184.
[53] G.T. Duan, W.P. Cai, Y.Y. Luo, F.Q. Sun, Adv. Funct. Mater. 17 (2007) 644.
[54] Y. Li, W.P. Cai, B.Q. Cao, G.T. Duan, F.Q. Sun, C.C. Li, L.C. Jia, Nanotechnology 17 (2006) 238.
[55] Y. Li, W.P. Cai, G.T. Duan, B.Q. Cao, F.Q. Sun, F. Lu, J. Colloid Interface Sci. 287 (2005) 634.
[56] Y. Li, G.T. Duan, W.P. Cai, J. Colloid Interface Sci. 314 (2007) 615.
[57] F. Yan, W.A. Goedel, Nano Lett. 4 (2004) 1193.
[58] G.T. Duan, W.P. Cai, Y.Y. Luo, Z.G. Li, Y. Lei, J. Phys. Chem. B 110 (2006) 15729.
[59] G.T. Duan, W.P. Cai, Y.Y. Luo, Y. Li, Y. Lei, Appl. Phys. Lett. 89 (2006) 181918.
[60] Y. Li, W.P. Cai, G.T. Duan, B.Q. Cao, F.Q. Sun, J. Mater. Res. 20 (2005) 338.
[61] Y. Li, C.C. Li, S.O. Cho, G.T. Duan, W.P. Cai, Langmuir 23 (2007) 9802.
[62] F.Q. Sun, W.P. Cai, Y. Li, B.Q. Cao, Y. Lei, L.D. Zhang, Adv. Funct. Mater. 14 (2004) 283.
[63] F.Q. Sun, J.C. Yu, X.C. Wang, Chem. Mater. 18 (2006) 3774.
[64] S.V. Kesapragada, D. Gall, Thin Solid Films 494 (2006) 234.
[65] C.M. Zhou, H.F. Li, D. Gall, Thin Solid Films 517 (2008) 1214.
[66] Y.-P. Zhao, D.-X. Ye, G.-C. Wang, T.-M. Lu, Nano Lett. 2 (2002) 351.
[67] C.M. Zhou, D. Gall, J. Vac. Sci. Technol. A 25 (2007) 312.
[68] Y.-P. Zhao, D.-X. Ye, P.-I. Wang, G.-C. Wang, T.-M. Lu, Int. J. Nanosci. Nanotechnol. 1 (2002) 87.
[69] C.M. Zhou, D. Gall, Thin Solid Films 515 (2006) 1223.
[70] C.M. Zhou, D. Gall, Small 4 (2008) 1351.
[71] C.M. Zhou, D. Gall Branched, Appl. Phys. Lett. 88 (2006) 203117.
[72] Y. Li, T. Sasaki, Y. Shimizu, N. Koshizaki, J. Am. Chem. Soc. 130 (2008) 14755.
[73] Y. Li, N. Koshizaki, Y. Shimizu, L. Li, S. Gao, T. Sasaki, ACS Appl. Mater. Interfaces 1 (2009) 2580.
[74] L. Li, N. Koshizaki, J. Mater. Chem. 20 (2010) 2972.
[75] L. Li, Y. Li, S. Gao, N. Koshizaki, J. Mater. Chem. 19 (2009) 8366.
[76] Y. Li, X. Fang, N. Koshizaki, T. Sasaki, L. Li, S. Gao, Y. Shimizu, Y. Bando, D. Golberg, Adv. Funct. Mater. 19 (2009) 2467.
[77] Y. Li, T. Sasaki, Y. Shimizu, N. Koshizaki, Small 4 (2008) 2286.
[78] J. Elias, C. Lévy-Clément, M. Bechelany, J. Michler, G.-Y. Wang, Z. Wang, L. Philippe, Adv. Mater. 22 (2010) 1607.
[79] G. Duan, F. Lv, W. Cai, Y. Luo, Y. Li, G. Liu, Langmuir 26 (2010) 6295.
[80] Y. Li, W.P. Cai, B.Q. Cao, G.T. Duan, F.Q. Sun, Polymer 46 (2005) 12033.
[81] H.B. Zeng, X.J. Xu, Y. Bando, U.K. Gautam, T.Y. Zhai, X.S. Fang, B.D. Liu, D. Golberg, Adv. Funct. Mater. 19 (2009) 3165.
[82] C. Li, G. Hong, P. Wang, D. Yu, L. Qi, Chem. Mater. 21 (2009) 891.
[83] C. Li, L.M. Qi, Adv. Mater. 22 (2010) 1494.
[84] L.M. Qi, Coord. Chem. Rev. 254 (2010) 1054.
[85] Y. Li, E.J. Lee, W. Cai, K.Y. Kim, S.O. Cho, ACS Nano 2 (2008) 1108.
[86] X.-J. Huang, Y. Li, Y.-K. Choi, J. Electroanal. Chem. 617 (2008) 218.

[87] Y. Li, E.J. Lee, S.O. Cho, J. Phys. Chem. C 111 (2007) 14813.
[88] X.J. Huang, Y. Li, H.S. Im, O. Yarimaga, J.H. Kim, D.Y. Jang, S.O. Cho, W.P. Cai, Y.-K. Choi, Nanotechnology 17 (2006) 2988.
[89] C.L. Cheung, R.J. Nikolić, C.E. Reinhardt, T.F. Wang, Nanotechnology 17 (2006) 1339.
[90] W.-L. Min, P. Jiang, B. Jiang, Nanotechnology 19 (2008) 475604.
[91] Z.Y. Ma, G.Y. Liu, M.Y. Yan, G.Y. Xia, X.F. Jiang, T. Ling, H.C. Sun, D.Q. Wang, H.P. Dong, L. Xu, W. Li, K.J. Chen, J. Xu, D. Feng, Phys. Status Solidi C 7 (2010) 739.
[92] W.Y. Fu, K.K.-Y. Wong, H.W. Choi, J. Appl. Phys. 107 (2010) 063104.
[93] B.-J. Kim, H. Jung, H.-Y. Kim, J. Bang, J. Kim, Thin Solid Films 517 (2009) 3859.
[94] S.G. Jang, H.K. Yu, D.-G. Choi, S.-M. Yang, Chem. Mater. 18 (2006) 6103.
[95] C.-W. Kuo, J.-Y. Shiu, P. Chen, Chem. Mater. 15 (2003) 2917.
[96] C.-W. Kuo, J.-Y. Shiu, P. Chen, G.A. Somorjai, J. Phys. Chem. B 107 (2003) 9950.
[97] C.-W. Kuo, J.-Y. Shiu, Y.-H. Cho, P. Chen, Adv. Mater. 15 (2003) 1065.
[98] A. Sinitskii, S. Neumeier, J. Nelles, M. Fischler, U. Simon, Nanotechnology 18 (2007) 305307.
[99] H.-Y. Hsieh, S.-H. Huang, K.-F. Liao, S.-K. Su, C.-H. Lai, L.-J. Chen, Nanotechnology 18 (2007) 505305.
[100] Z.P. Huang, D.L. Carnahan, J. Rybczynski, M. Giersig, M. Sennett, D.Z. Wang, J.G. Wen, K. Kempa, Z.F. Ren, Appl. Phys. Lett. 82 (2003) 460.
[101] Y. Wang, J. Rybczynski, D.Z. Wang, K. Kempa, Z.F. Ren, W.Z. Li, B. Kimball, Appl. Phys. Lett. 85 (2004) 4741.
[102] K. Kempa, B. Kimball, J. Rybczynski, Z.P. Huang, P.F. Wu, D. Steeves, M. Sennett, M. Giersig, D.V.G.L.N. Rao, D.L. Carnahan, D.Z. Wang, J.Y. Lao, W.Z. Li, Z.F. Ren, Nano Lett. 3 (2003) 13.
[103] J. Rybczynski, K. Kempa, Y. Wang, Z.F. Ren, J.B. Carlson, B.R. Kimball, G. Benham, Appl. Phys. Lett. 88 (2006) 203122.
[104] K.H. Park, S. Lee, K.H. Koh, R. Lacerda, K.B.K. Teo, W.I. Milne, J. Appl. Phys. 97 (2005) 024311.
[105] P. Wu, B. Kimball, J. Carlson, V.G.L.N. Rao, Phys. Rev. Lett. 93 (2004) 013902.
[106] T. Xu, J. Miao, M. Ashraf, N. Lin, F. Chollet, Mater. Lett. 63 (2009) 867.
[107] K. Ryu, A. Badmaev, L. Gomez, F. Ishikawa, B. Lei, C. Zhou, J. Am. Chem. Soc. 129 (2007) 10104.
[108] Z.S. Houweling, V. Verlaan, G.T. ten Grotenhuis, R.E.I. Schropp, Thin Solid Films 517 (2009) 3566.
[109] X.D. Wang, C.N.E. Graugnard, Y. Ding, J.S. King, L.A. Pranger, R. Tannenbaum, Z.L. Wang, C.J. Summers, Adv. Mater. 17 (2005) 2103.
[110] X.D. Wang, C.J. Summers, Z.L. Wang, Nano Lett. 4 (2004) 423.
[111] X.D. Wang, J.H. Song, Z.L. Wang, J. Mater. Chem. 17 (2007) 711.
[112] H.J. Fan, B. Fuhrmann, R. Scholz, F. Syrowatka, A. Dadgar, A. Krost, M. Zacharias, J. Cryst. Growth 287 (2006) 34.
[113] D. Banerjee, J. Rybczynski, J.Y. Huang, D.Z. Wang, K. Kempa, Z.F. Ren, Appl. Phys. A 80 (2005) 749.
[114] D.F. Liu, Y.J. Xiang, X.C. Wu, Z.X. Zhang, L.F. Liu, L. Song, X.W. Zhao, S.D. Luo, W.J. Ma, J. Shen, W.Y. Zhou, G. Wang, C.Y. Wang, S.S. Xie, Nano Lett. 6 (2006) 2375.
[115] D.F. Liu, Y.J. Xiang, Q. Liao, J.P. Zhang, X.C. Wu, Z.X. Zhang, L.F. Liu, W.J. Ma, J. Shen, W.Y. Zhou, S.S. Xie, Nanotechnology 18 (2007) 405303.
[116] B. Fuhrmann, H.S. Leipner, H.-R. Höche, L. Schubert, P. Werner, U. Gösele, Nano Lett. 5 (2005) 2524.
[117] G. Radhakrishnan, A. Freundlich, B. Fuhrmann, J. Cryst. Growth 311 (2009) 1855.
[118] C.M. Zhou, D. Gall, Appl. Phys. Lett. 90 (2007) 093103.
[119] C.M. Zhou, D. Gall, Thin Solid Films 516 (2007) 433.
[120] J.-H. Lee, Y.-W. Chung, M.-H. Hon, I.-C. Leu, Appl. Phys. A 97 (2009) 403.
[121] X.H. An, G.W. Meng, Q. Wei, M.G. Kong, L.D. Zhang, J. Phys. Chem. B 110 (2006) 222.
[122] T.-Y. Tsai, T.-H. Chen, N.-H. Tai, S.-C. Chang, H.-C. Hsu, T.J. Palathinkal, Nanotechnology 20 (2009) 305303.
[123] K.-C. Hsieh, T.-Y. Tsai, D. Wan, H.-L. Chen, N.-H. Tai, ACS Nano 4 (2010) 1327.
[124] S.M. Weekes, F.Y. Ogrin, W.A. Murray, Langmuir 20 (2004) 11208.
[125] Z. Huang, H. Fang, J. Zhu, Adv. Mater. 19 (2007) 744.
[126] K. Peng, M. Zhang, A. Lu, N.-B. Wong, R. Zhang, S.-T. Lee, Appl. Phys. Lett. 90 (2007) 163123.
[127] A. Ladenburger, A. Reiser, J. Konle, M. Feneberg, R. Sauer, K. Thonke, F. Yan, W.A. Goedel, J. Appl. Phys. 101 (2007) 034302.
[128] P. Jiang, Langmuir 22 (2006) 3955.
[129] M.-J. Huang, C.-R. Yang, R.-T. Lee, Y.-C. Chiou, J. Micromech. Microeng. 19 (2009) 045003.
[130] A. Nakajima, K. Hashimoto, T. Watanabe, Monatsh. Chem. 132 (2001) 31.
[131] T. Sun, L. Feng, X. Gao, L. Jiang, Acc. Chem. Res. 38 (2005) 644.
[132] X.-M. Li, D. Reinhoudt, M. Crego-Calama, Chem. Soc. Rev. 36 (2007) 1350.
[133] X.-J. Huang, J.-H. Lee, J.-W. Lee, J.-B. Yoon, Y.-K. Choi, Small 4 (2008) 211.
[134] X.-J. Huang, D.-H. Kim, M. Im, J.-H. Lee, J.-B. Yoon, Y.-K. Choi, Small 5 (2008) 90.
[135] Y. Li, X.J. Huang, S.H. Heo, C.C. Li, Y.K. Choi, W.P. Cai, S.O. Cho, Langmuir 23 (2007) 2169.
[136] R.N. Wenzel, J. Phys. Colloid Chem. 53 (1949) 1446.
[137] R. Wang, K. Hashimoto, A. Fujishima, M. Chikuni, E. Kojima, A. Kitamura, M. Shimohigoshi, T. Watanabe, Adv. Mater. 10 (1998) 135.
[138] W.-L. Min, B. Jiang, P. Jiang, Adv. Mater. 20 (2008) 3914.
[139] Y. Li, J. Zhang, S. Zhu, H. Dong, Z. Wang, Z. Sun, J. Guo, B. Yang, J. Mater. Chem. 19 (2009) 1806.
[140] Y.-R. Lin, H.-P. Wang, C.-A. Lin, J.-H. Hea, J. Appl. Phys. 106 (2009) 114310.
[141] S.S. Fan, M.G. Chapline, N.R. Franklin, T.W. Tombler, A.M. Cassell, H.J. Dai, Science 283 (1999) 512.
[142] X.S. Fang, Y. Bando, U.K. Gautam, C.H. Ye, D. Golberg, J. Mater. Chem. 18 (2008) 509.
[143] R.H. Fowler, L.W. Nordheim, Proc. R. Soc. Lond., Ser. A 119 (1928) 173.
[144] R.H. Lipson, C. Lu, Eur. J. Phys. 30 (2009) S33.
[145] Y.-C. Chang, H.-W. Wu, H.-L. Chen, W.-Y. Wang, L.-J. Chen, J. Phys. Chem. C 113 (2009) 14778.
[146] V.P. Khostikov, O.A. Khvostikova, P.Y. Gazaryan, S.V. Sorokina, N.S. Potapovich, A.V. Malevskaya, N.A. Kaluzhniy, M.Z. Shvarts, V.M. Andreev, J. Sol. Energy Eng. 129 (2007) 291.
[147] P.B. Clapham, M.C. Hutley, Nature (Lond.) 244 (1973) 281.
[148] D.G. Stavenga, S. Foletti, G. Palasantzas, K. Arikawa, Proc. R. Soc. Lond., Ser. B 273 (2006) 661.
[149] C.-H. Sun, P. Jiang, B. Jiang, Appl. Phys. Lett. 92 (2008) 061112.
[150] W.-L. Min, A.P. Betancourt, P. Jiang, B. Jiang, Appl. Phys. Lett. 92 (2008) 141109.
[151] C.-H. Sun, B.J. Ho, B. Jiang, P. Jiang, Opt. Lett. 33 (2008) 2224.
[152] H. Xu, N. Lu, D. Qi, L. Gao, J. Hao, Y. Wang, L. Chi, Microelectr. Eng. 86 (2009) 850.
[153] B.-J. Kim, J. Bang, S.H. Kim, J. Kim, Korean J. Chem. Eng. 27 (2010) 693.
[154] C.-Y. Wang, L.-Y. Chen, C.-P. Chen, Y.-W. Cheng, M.-Y. Ke, M.-Y. Hsieh, Opt. Express 16 (2008) 10549.
[155] L.-Y. Chen, Y.-Y. Huang, C.-H. Chang, Y.-H. Sun, Y.-W. Cheng, M.-Y. Ke, C.-P. Chen, J.J. Huang, Opt. Express 18 (2010) 7664.